Spring 2019

Three-Dimensional Echocardiographic Analysis of the Equine Aortic Valve

Amber McElhinney
University of New Hampshire, Durham

Three-Dimensional Echocardiographic Analysis of the Equine Aortic Valve

Amber McElhinney

Thesis Advisors: Dr. John Keen, Dr. Drew Conroy, Dr. Pete Erickson

Honors Senior Thesis, 2019

Contents

Table of Figures

Acknowledgements

First and foremost, I would like to thank my faculty mentor Dr. Drew Conroy for telling me about the Summer Undergraduate Research Fellowship (SURF) Abroad and helping me with everything from putting a proposal together to actually writing up my research. Thank you to Dr. John Keen, who allowed me to work with him in Scotland and taught me about equine cardiology. Thank you to PhD candidates Jenny Brown and Rachel Jago for taking me under their wings while abroad and teaching me practical skills while I assisted on their study. Thank you to my adviser Sarah Rigg for being supportive of everything I do and writing me countless recommendation letters throughout my time at UNH. Thank you to Dr. Pete Erickson for helping me to statistically analyze my data. To my friends and family—thank you for listening about my research, even when you had no idea what I was talking about. Finally, thank you to everyone at the Hamel Center for Undergraduate Research for making my research possible, especially Dr. Georgeann Murphy for organizing everything and keeping in touch throughout the summer, and Mr. Dana A. Hamel and Mr. Benjamin Marcek for funding my research.

Abstract

This research focused on 3D echocardiography of the aortic valve (AV) in horses. Aortic regurgitation (AR) can be a common finding in older horses, and in severe cases can result in decreased performance and even sudden cardiac death. Standard AR diagnosis includes 2D echocardiography from the right side of the horse. Three-dimensional echocardiography (3DE) records a pyramid of tissue, showing structures in the heart difficult to visualize in 2D methods, and can be more accurate as it does not rely as heavily on placement of the transducer. Nine images of normal AV's were assessed, and still frames of anatomical structures were obtained. Area and circumference from the enface view, and diameter and cusp thicknesses from side and enface views were measured. These measurements were also taken on images from 5 horses with mild, 7 with moderate, and 2 with severe AR. 3DE images from the left side of 9 normal horses were taken for comparison. In normal valves, the edges of the cusps were visible but the centers were not from the right. The left coronary cusp was generally most visible from the right sided view. The cusp edges and lunulae of the aortic valve were thickened in horses with AR, with degree of thickening corresponding to AR severity. The center of the cusps appeared opaque in some horses with AR. There was a statistically significant positive correlation between thickness of the left coronary cusp and AR severity. Left sided images were generally of worse quality than those from the right, but in some cases there was better visualization of the right and noncoronary cusps. 3DE could potentially be used as a standard for diagnosis of AR, specifically by looking at cusp thicknesses, and could more specifically diagnose which part of the valve is affected by disease.

Introduction

Anatomy

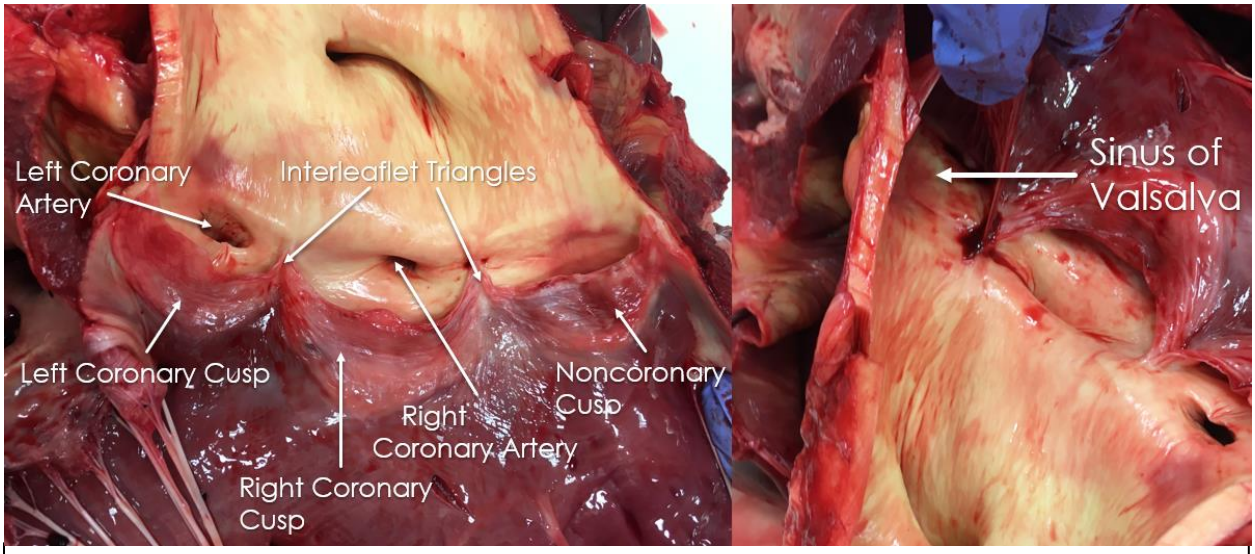

Figure 1: A dissected aortic root from a 9 year old Irish Sport Horse. The cut for this dissection was made between the LCC and NCC, which in a live heart would be attached to form the bulbous structure of the aortic root. All cusps, interleaflet triangles, sinuses of Valsalva and coronary arteries are shown. In the image on the right, the NCC is lifted to show the corresponding sinus of Valsalva.

The aortic valve is one of the semilunar valves, the other being the pulmonary valve, and is between the left ventricle and the aorta. It is fitted within the circular short axis profile of the left ventricle next to the mitral valve (Anderson R. , 2000). It allows blood to flow from the heart to the rest of the body, and as such is subject to both arterial and ventricular pressure (Anderson R. , 2000). It is made up of three cusps or leaflets: the left coronary cusp (LCC), right coronary cusp (RCC), and non-coronary cusp (NCC), which are attached to the aortic root by semilunar attachments. The NCC is positioned superior to the interventricular septum, somewhat between the septum and the mitral valve. The LCC is also proximal to the mitral valve on the left, and the RCC is closest to the right side of the heart. During diastole the leaflets are closed to allow the left ventricle to fill, and during systole they are open to allow blood to be pumped through. The commissure is where the cusps meet when the valve closes (Sutton, Ho, & Anderson, 1995).

When closed, the cusps overlap slightly. This overlapping surface is called the lunula (Sutton, Ho, & Anderson, 1995).

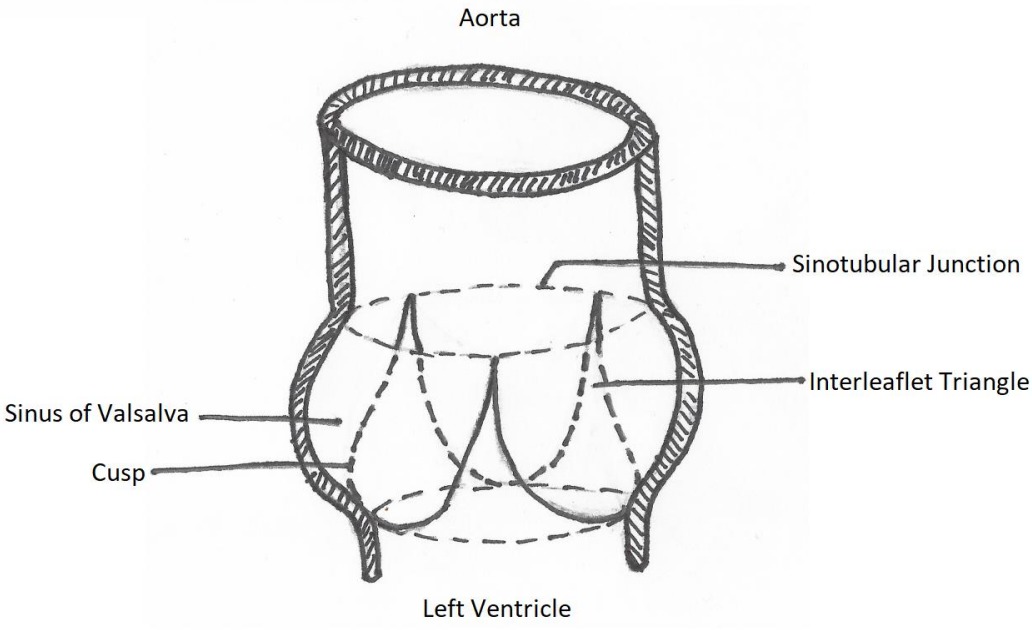

Figure 2: A diagram of the structure of the aortic root adapted from Sutton, Ho, & Anderson, 1995. This shows the layout of the valve as it would be in a live, functioning heart.

Cardiac valve shape is classically described as an annulus, or ring-like structure. This term is controversial in the aortic valve, as it is not a true ring but rather a three-dimensional crown-like structure due to the semilunar nature of the cusp attachments. (Anderson R. , 2000). The cusps open into the sinuses of Valsalva corresponding in name (Sutton, Ho, & Anderson, 1995). The left and right coronary aortic sinuses give rise to the left and right coronary arteries, respectively, at or below the sinotubular junction (Anderson R. , 2000). The sinuses are made up mostly of the aorta wall, with ventricular musculature at the base in the right and left coronary sinuses (Anderson R. , 2000). The noncoronary sinus has a fibrous base due to its proximity to the mitral valve, and the continuity of the valvar leaflets (Anderson R. , 2000). Between each of the sinuses is a triangular extension of the left ventricular outflow tract (LVOT). These are called

the interleaflet triangles, and are bound by the thin fibrous aorta walls between the expanded sinuses (Anderson R. , 2000). They allow each of the sinuses to function independently (Sutton, Ho, & Anderson, 1995). The sinotubular junction is the top of the valvular sinuses, at the superior point of the interleaflet triangles. This is where the sinuses meet the tubular structure of the ascending aorta, hence the name sinotubular junction.

Disease

Aortic Regurgitation (AR) is one disease commonly seen in the aortic valve in horses It is described as blood flowing back into the left ventricle during diastole, and creates inefficiency of cardiac function, as not all blood is being pumped back into the body. It is common in older horses, but when detected in younger horses, especially less than ten years of age, is a cause for particular concern (Jago & Keen, 2017). Prognosis depends on severity of disease and work load of the horse. Routine monitoring of the condition is indicated in all cases to ensure that the condition is not worsening with work load.

Common causes of AR include degenerative valve thickening, aortic valve prolapse, congenital malformations, cusp tears, infective endocarditis, valvulitis, fenestrations, aortic root disease, and some ventricular septal defects (VSD) can also result in AR (Reef, et al., 2014). In mild cases this can be asymptomatic, but in severe cases can lead to sudden cardiac death. Murmurs associated with AR are often detected incidentally, and a left-sided holodiastolic murmur is indicative of AR unless proven otherwise (Reef, et al., 2014). On auscultation, a murmur from AR is generally of longer duration than a similarly located murmur from physiological filling (Jago & Keen, 2017). Bounding hyperdynamic arterial pulses suggest hemodynamically severe AR with left ventricle (LV) volume overload (Reef, et al., 2014). Once the left atrium is enlarged, the risk of Atrial Fibrillation (AF), pulmonary hypertension, and

congestive heart failure increase (Reef, et al., 2014). When mild, AR is often associated with normal life expectancy and performance. The first noticeable sign of progressing AR is usually decreased performance. Chronic AR leads to an enlargement of the left ventricle from volume overloading. Thickening of the aortic valve can occur in conjunction with AR, and on 2D echocardiography can appear as a fibrous band-like lesion (Reef, et al., 2014). In one study, the cusp most commonly thickened due to AR was the LCC (Reef & Spencer, 1987). The enlargement of the left ventricle can then lead to ventricular arrhythmias or AF. These arrhythmias can sometimes be fatal, and sudden cardiac death is possible as a result (Reef, et al., 2014). There is a period before signs of cardiac failure where horses with severe AR are at an increased risk of sudden cardiac death or collapse (Young L. , 2007). This is because exercise-induced ventricular arrhythmias can occur that are not detectable at rest. This occurs during periods of ischemia, or during decreased blood and oxygen supply, when there is an increased excitability of the myocardial cells (Young L. , 2007). The excitability of the myocardial cells leads to fibrillation, which can then cause sudden cardiac death.

The possibility for sudden cardiac death in AR is cause for the need of more accurate predictions of AR severity. Better classification of AR could help to reduce human injury and equine mortality from a horse experiencing sudden cardiac death. In general, prognosis is assumed to be good if the AR is mild and there are few changes on follow up examinations (Reef, et al., 2014). In more severe cases, horses may need to be taken down a level in work or retired if heart failure is a concern.

Overview of Imaging/Echocardiography

Echocardiography is ultrasonography of the heart and can be used as a diagnostic tool for various cardiac conditions. Ultrasound uses sound waves to create images of internal soft-tissue structures. Some clinically used types of echocardiography are Doppler, motion mode, and two-dimensional (Gazi, et al., 2015). Doppler echocardiography shows velocity, direction, and patterns of blood flow (Gazi, et al., 2015). It measures frequency changes, known as the Doppler shift, as ultrasound waves reflect off of individual blood cells, allowing blood flow velocity to be calculated when the ultrasound beam is parallel to the blood flow (Gazi, et al., 2015). Deviations from parallel reduce the accuracy of Doppler evaluation, making human error an issue in the exactness of this evaluative method. There are two types of Doppler echocardiography: pulse wave and continuous wave. Pulse wave uses short ultrasound bursts to a designated point, allowing blood flow direction, velocity, and spectral characteristics to be calculated for specific points in the heart, but limiting the maximum measurable blood flow velocity (Gazi, et al., 2015). Continuous wave Doppler echocardiography utilizes dual crystals, or two crystals in the transducer instead of one, allowing the simultaneous receiving and sending of ultrasound waves (Gazi, et al., 2015). The advantage to this method is that there is no maximum measurable velocity, but the disadvantage is that data is collected along the entire ultrasound beam, not in one specified area (Gazi, et al., 2015). In Doppler echocardiography, color is used to map blood flow in the heart, and may show areas where blood flow is too fast (Gazi, et al., 2015). This can aid in the diagnosis of disorders such as subaortic stenosis or pulmonary stenosis, defects which cause narrowing in the affected valves, as well as detect leakage of heart valves (Gazi, et al., 2015). However, it can also detect valvular regurgitation in horses without murmurs (Marr & Bowen, Cardiology of the Horse, 2010). Therefore, it is sensitive enough to pick up on

regurgitation that is not necessarily clinically significant, assuming correct and parallel beam placement.

Motion mode echocardiography provides a one-dimensional view of the heart over time (Gazi, et al., 2015). This type of echocardiography does not display an image of the heart, but rather recorded lines which correspond to the position of the imaged structures in relation to other cardiac structures and the transducer (Gazi, et al., 2015). It is essentially a graph of a single line of tissue versus distance from the probe over time. The high sampling rate of this method allows for cleaner cardiac borders, more accurate dimensions of cardiac anatomy, and more critical evaluation of cardiac motion (Gazi, et al., 2015). In veterinary medicine, standard motion mode views include the left ventricle, mitral valve, and aortic root (Gazi, et al., 2015). Two-dimensional echocardiography shows both depth and width of a plane of tissue in real time, allowing for easier comprehension of the anatomical relationships between different structures (Gazi, et al., 2015). While there is no limit to the possible imaging planes with this method, the most commonly used in large animal medicine include short axis views of the left ventricle, mitral valve, aorta and left atrial appendage, as well as long axis views of the mitral valve, aorta, and pulmonary artery (Gazi, et al., 2015). Both of these techniques are currently used for imaging the aorta, as described above, although they each have their own limitations.

Three-dimensional echocardiography (3DE) is a fairly new technology, and there are not yet standards for its use in assessment of the equine aortic valve (Keen, 2016). Prototypes of this technology were created in the early 1990's, and its progression into mainstream diagnostic techniques has been slow (Chien-Chia Wu & Takeuchi, 2017). Initially, analysis of two-dimensional echocardiograms was required to construct three-dimensional views of the heart (Chien-Chia Wu & Takeuchi, 2017). These views can now be observed in real time, without

having to wait to reconstruct the images later, utilizing modern technology. Real time three-dimensional echocardiography allows medical professionals to visualize cardiac structures with depth and obtain more accurate quantification of volumes and structure size, as these measurements are not dependent on geometric calculations (Chien-Chia Wu & Takeuchi, 2017). For example, the left ventricular outflow tract has been seen to be ellipsoidal in shape, rather than circular as geometrically assumed with two-dimensional echocardiographic techniques (Chien-Chia Wu & Takeuchi, 2017). This shape discrepancy was also true of the vena contracta area of aortic regurgitation (Chien-Chia Wu & Takeuchi, 2017). A more comprehensive view of the heart and specific structures in clinical settings could help make diagnosis of cardiac disorders easier and more accurate.

In 3DE, a pyramid of tissue is recorded rather than a flat 2D image. This pyramid can then be analyzed on computer software, rotated and settings adjusted to view any portion within the recorded area. The gain settings can be adjusted both before and after taking the image to enhance image quality. Increasing the gain essentially increases the signal received by the transducer, therefore making the image brighter. As ultrasound makes an image from sound waves, gain is essentially synonymous to a volume adjustment. Another basic consideration when taking echocardiograms of any modality is frame rate. Frame rate is the number of frames per second recorded and is inversely proportional to image resolution. While increasing frame rate may allow one to see a more complete picture cardiac motion and potentially related abnormalities, the image quality itself will worsen. Other factors that influence image quality and clarity are depth and width of the image. The deeper into the body that is being imaged, the weaker the signal is that bounces back and therefore the lower the image quality. Likewise, the wider the area one is imaging, the more spread out the signal and therefore the lower quality the

image. These are especially issues in horses, where their bodies are so large that the heart is both a large area to image and it is deep within the body. One way to correct for this is by taking the image in multi-beat, which records one cardiac cycle of a smaller section of tissue, then one of the adjacent section, etc. until the whole desired section of tissue has been recorded for one cardiac cycle. These smaller sections are then stitched together by the ultrasound machine to form one image. This allows for larger sections of tissue to be recorded with higher resolution. However, since each section was recorded at a different time, there can sometimes be stitch artifacts in the image. The heart does not always move in exactly the same way for each beat, so when multiple beats are put together there can be overlap of some sections of tissue. This means that there can be inaccuracies in the image which can therefore impede accurate evaluation of the valve.

Currently, three-dimensional echocardiographic technology is available but not commonly found in clinical settings. Diagnoses of cardiac conditions are based on standards that have been developed with conventional methods of echocardiography, such as 2D and Doppler. 3D technology is most prevalent in teaching hospitals (Hallowell & Bowen, 2013), as it shows a more comprehensive view of the heart, making it easier for students to view cardiac structures. It could be a very useful diagnostic tool in clinical settings, but standards for use and views are not commonly available. These standards need to be studied and determined for all structures in the heart before this technology can become common in veterinary practice (Keen, 2016).

3DE is not a standard used in diagnosis of aortic valve disease in horses. Current methods include M-Mode and 2D echocardiography of the aorta from right parasternal transthoracic views to measure diameter of the aorta (Marr & Bowen, Cardiology of the Horse, 2010). These methods, along with Doppler echocardiography, are also used to identify forms of valvular

pathology, determine the severity of the regurgitation, and document size and shape of vessels and cardiac chambers (Marr & Bowen, Cardiology of the Horse, 2010).

Materials/Methods

A catalog of all cardiac cases at the University of Edinburgh Royal (Dick) School of Veterinary Studies Equine Hospital from 2010 to 2018 was established in Microsoft Excel, with details including horse name, patient ID, age, weight, breed, color, and sex of the horse, date the image was taken, referral reasons, and final diagnosis. All cases involving aortic regurgitation were also filed in a separate Excel sheet. These images were taken from right parasternal transthoracic long axis views. All images in this study were taken using a GE Vivid E9 Ultrasound system with an active matrix 4D volume phased array transducer (3V-D probe). All image analyses and measurements were done with GE EchoPac software on the volume rendering screen for 4D image analysis. The volume rendering image is the 3D image used for analysis, while the 2D images of two planes in the 3D image, from now on referred to as the cut planes, were used as reference points for views and image analysis. The dashed yellow line through the cut planes delineated what was being cropped out of the images for each view taken, and will be referred to as the crop plane.

Cardiac scans of forty Thoroughbred horses with normal cardiac function had been taken in April 2015, including 3D images of the aorta. These images were sorted through and subjectively graded from 1-3, with 3 being ideal and 1 being unusable. Each image was assessed on the frame rate, whether it was a complete view of the aortic root, whether it was multi beat, the severity of stitch artifacts if multi beat, image quality, and motion quality. Images with frame rates lower than 5 or 6 were generally unusable and poor quality. Higher frame rates were preferred, but many of the images with high frame rates in the 30’s or 40’s had stitch artifacts

which lessened the quality of the image and impeded visualization of the aortic valve. Multi-beat images were subjectively graded on their stitch artifacts, with 1 being not noticeable or not affecting the image, 2 having a moderate effect on the image, and 3 severely affecting the appearance of the valve. Some images had stitch artifacts that were only present at certain times in the cardiac cycle, and these were judged according to whether useful still images could be obtained. Image quality was assessed on how grainy the image appeared, how dark or light, and how well the valve cusps could be visualized. Motion quality was assessed on how smooth or jumpy the motion appeared during the cardiac cycle. Images that had good motion and image quality along with no or minor stitch artifacts were generally considered ideal and were given a mark of 3. There were 9 images found to be of good quality, which were further analyzed to get a sense of what a normal equine aorta should look like on 3D echocardiography.

Each image was manipulated to get good still enface views in diastole and systole so that the valve cusps were as visible as possible. The 2D cut plane images were used as guides for where to view the valve from but were not always reliable. The angle from which images were taken varied slightly for each horse, so there was not a standard placement or angle of the crop plane that could be used for all assessments. The placement of the crop plane was kept relatively consistent within each horse in relation to the valve and related structures. If a good 2D side view of the valve was available, the crop plane was placed parallel to the valve leaflets in diastole, in the widest part of the aortic root. In systole the crop plane was placed at a similar point relative to the valve. Since the valve would often move during the cardiac cycle, the crop plane could not be left at the same point as in diastole (Figure 3). Color and gain settings were adjusted to provide the best visualization of aortic root structures.

Figure 3: Still images of the aortic valve of National Hunt racehorse "Ultra" in systole (right) and diastole (left). Long axis 2D view of aortic root is shown in top left corner of each, with crop plane (dashed yellow line) shown transecting similar points in the valve in systole and diastole. Yellow arrow indicates where volume rendering image (colored image to right) is viewed from in relation to 2D cross sections. Bright yellow arrow indicates view point is in front of 2D cross section, and dark yellow indicates behind cross section. Everything between the crop plane and arrow is cut out of volume rendering image.

Several novel measurements were taken, all in cm or cm^2. Measurements of the visible tissue between each of the leaflets, which included the lunulae and any visible surrounding tissue, were taken in diastole. This was deemed the "commissural measurement," as it was not necessarily a measurement of only the lunulae. This was done using the Caliper (Crop Plane) measurement tool in EchoPac by measuring from one end of visible tissue to the other towards the middle of the cusp (Figure 4). This was done to avoid artificially large measurements that could occur if taken towards the center or edge of the valve, as these had thickened appearances.

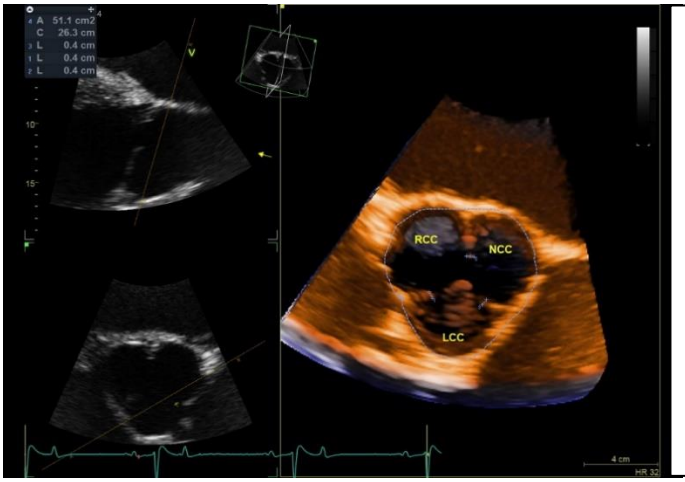

Figure 4:

Example of commissural measurements in the center of the valve, and area/circumference measurement around the edge of the valve shown in blue dashed lines on volume rendering image. Measurements taken on image of thoroughbred "Mac." The cusps are labeled in yellow.

The thickness of each cusp was also measured from a side view, taking measurements towards the center of each leaflet (Figure 5).

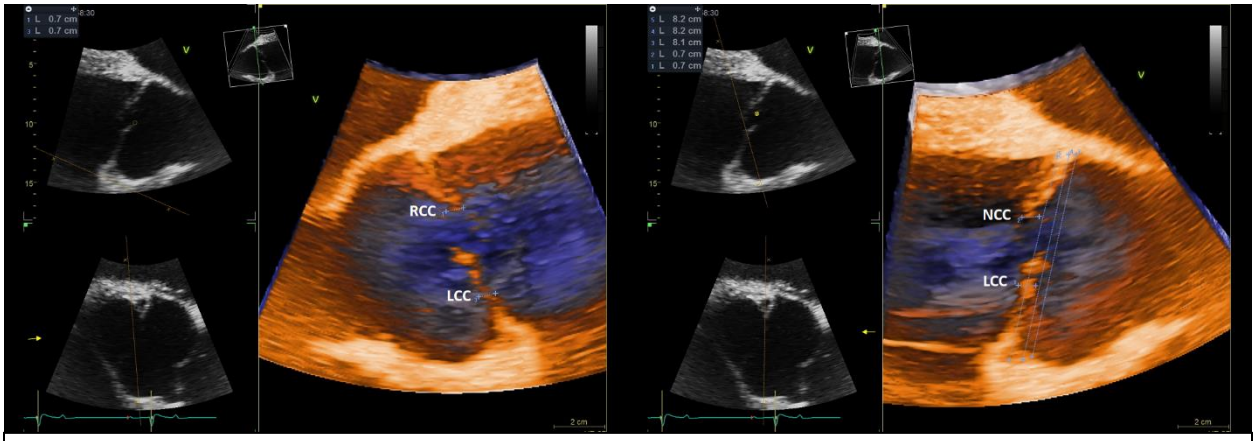

Figure 5: Example of cusp thickness measurements taken from each side view, one which contained the LCC and RCC (left) and the other the NCC and LCC (right). Diameter of the valve in diastole was also taken from this view (right). Valve images are from jump racing thoroughbred "Ultra." Valve cusps are labeled in white, and measurements are shows with blue dashed lines.

Area and circumference of the valve were taken in systole and diastole, as well as valve diameter from the front and from a side view. All diameter, area and circumference measurements were repeated three times and the averages were calculated. Area and circumference were measured by tracing the inside of the aorta using the Area (Crop Plane) tool in EchoPac on enface views of the valve (Figure 4). Diameter in diastole from the enface view was measured using the Caliper (Crop Plane) tool by measuring from the central edge of each cusp and through the opposing commissure (Figure 6). Diameters in systole were measured from similar places in the valve, making sure to go past the LCC seen at the bottom (Figure 6). Diameters from the side were taken in systole and diastole by measuring across the leaflets from the point of attachment of one to the other (Figures 5, 7). In addition to these novel measurements, good views of the interleaflet triangles, coronary arteries, and cusps were

obtained when possible from each image. 2D and 4D gain, color, and crop settings were adjusted accordingly to obtain the best images of various structures.

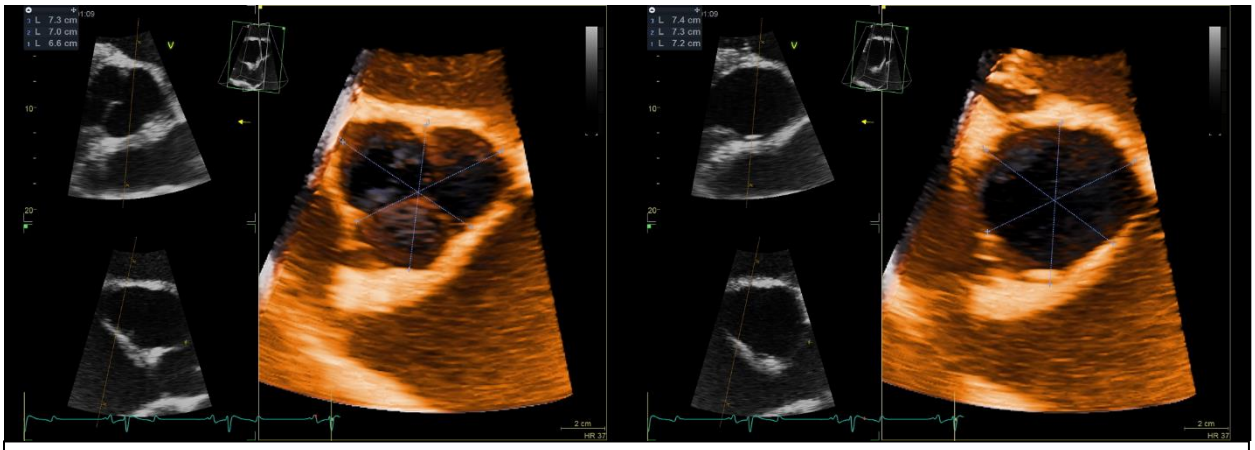

Figure 6: Example from thoroughbred "Thorpe" of measurements shown in blue dashed lines of valve diameter taken in diastole (left) and systole (right) from an enface view.

The same procedure was followed on the established cases of AR. 3D images of the aorta were similarly graded, and the best views were further analyzed. The images were separated by diagnosed severity of AR: mild, moderate, or severe. Where possible, one image from each visit was analyzed in horses that had follow-up visits. 21 images from 14 different horses were deemed of good quality; 6 had mild AR, 6 had moderate AR, and 2 had severe AR from endocarditis. The same measurements were taken as with the normal aortas for each image. Likewise, each image was manipulated to get good views of various anatomical structures, as

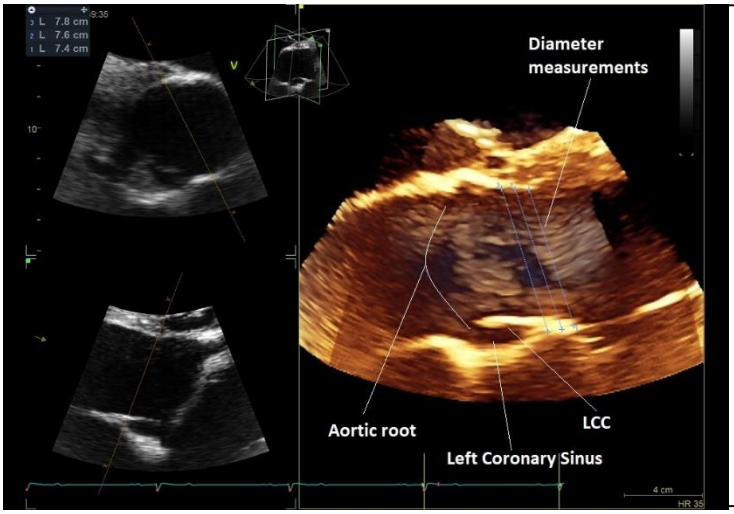

Figure 7: Image from racing thoroughbred "Ben" showing a side view of the aortic valve in systole. The Left Coronary Cusp can be seen it its open position, and the Left Coronary Sinus can be seen beneath it. The blue dashed lines indicate the three diameter measurements of the valve that were taken in systole. These were then averaged together to obtain the diameter of the valve in systole,

well as any pathology of the valve. The averaged measurements for mild and moderate AR were compared to the normal values. Values from the two horses with endocarditis were compared to normal, mild, and moderate AR. All measurements were analyzed using Statistical Analysis Software (SAS) to determine whether findings were significant.

9 horses with normal aortas were scanned from the left in an attempt to get clear views of the valve and leaflets. These were compared to the right views of normal aortas previously taken. Right parasternal long axis views were taken first, then left parasternal long axis views. These images taken from the left were compared to normal and abnormal views that had previously been taken from the right to determine visible anatomy from the left, and potential diagnostic usefulness in cardiac assessments.

Results

Normal Echocardiographic Anatomy from the Right Hemithorax

Transthoracic right parasternal 3D images of the aorta can be manipulated in a variety of ways to show many of the structures in the aortic root. From an enface view in diastole, the left coronary cusp was always at the bottom furthest from the transducer, while the noncoronary cusp was on the upper right and the right coronary cusp was on the upper left (Figure 8). The cusps themselves were not widely visible, but small sections of tissue, likely the lunulae, between

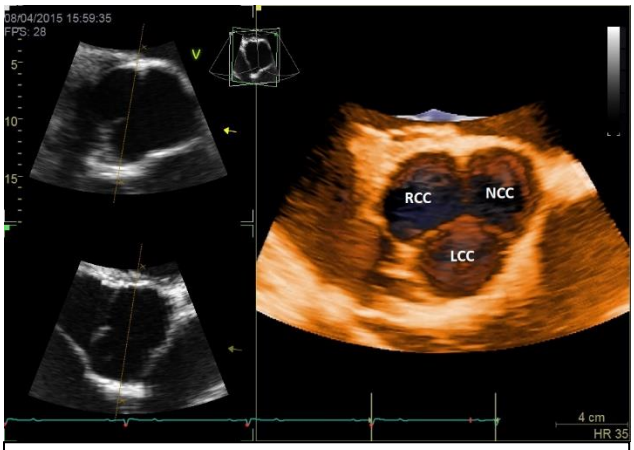

Figure 8: enface view of the aortic valve closed in diastole from Thoroughbred "Ben." This shows the location of each cusp when the valve is oriented with the apex of the image, or the point closest to the transducer, at the top of the screen, and the base at the bottom. This view is looking down at the top of the valve, with the left ventricle on the other side of the closed valve.

each cusp were visible. The left coronary cusp was generally more visible than the others, having a more opaque appearance throughout the center of the leaflet. Likewise, the tissue between the LCC and the other cusps was more visible than the tissue between the NCC and RCC. When the enface image was rotated to either side, with the crop plane between the NCC and RCC through the center of the LCC, cross sections of the valve leaflets could be viewed. When rotated left, the LCC and RCC were visible, while the LCC and NCC were visible when rotated right (Figure 5). Similar to the enface view, the LCC has a more uniform, opaque appearance, while the NCC and RCC were not as visible. The LCC was not necessarily thickened, it was just visible throughout the leaflet whereas the others were sometimes only visible in certain parts. This image could then be rotated up slightly to view the sinuses of Valsalva and the interleaflet triangles between the LCC and RCC or NCC (Figure 9). If the enface view was rotated up, the right coronary and noncoronary sinuses of Valsalva were visible. The crop plane could be adjusted to visualize various depths of the sinuses, or the outflow path of the right coronary artery (Figure 10).

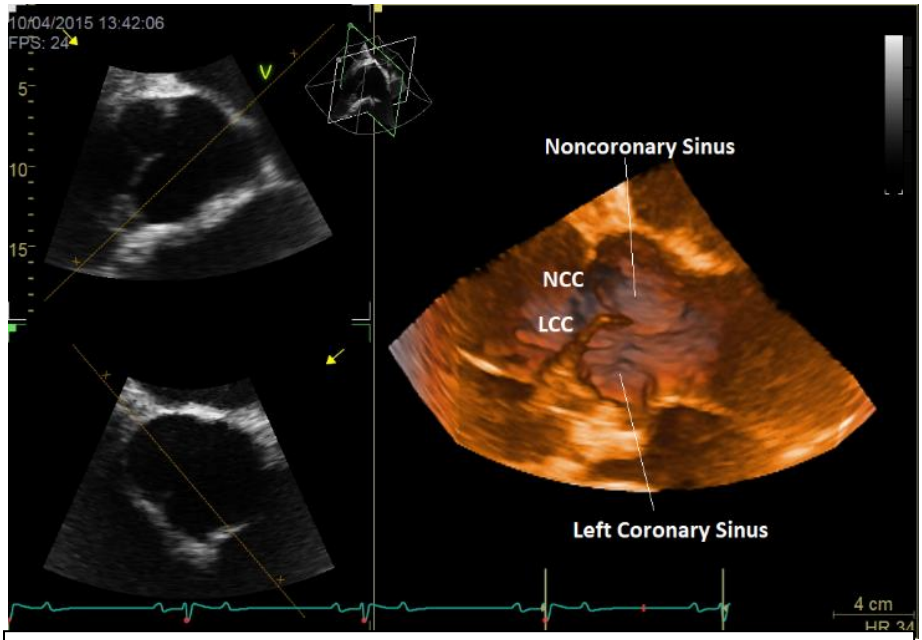

Figure 9: Image from Thoroughbred "Ryton." The right side view of the valve was rotated up to visualize the Left and Noncoronary Sinuses.

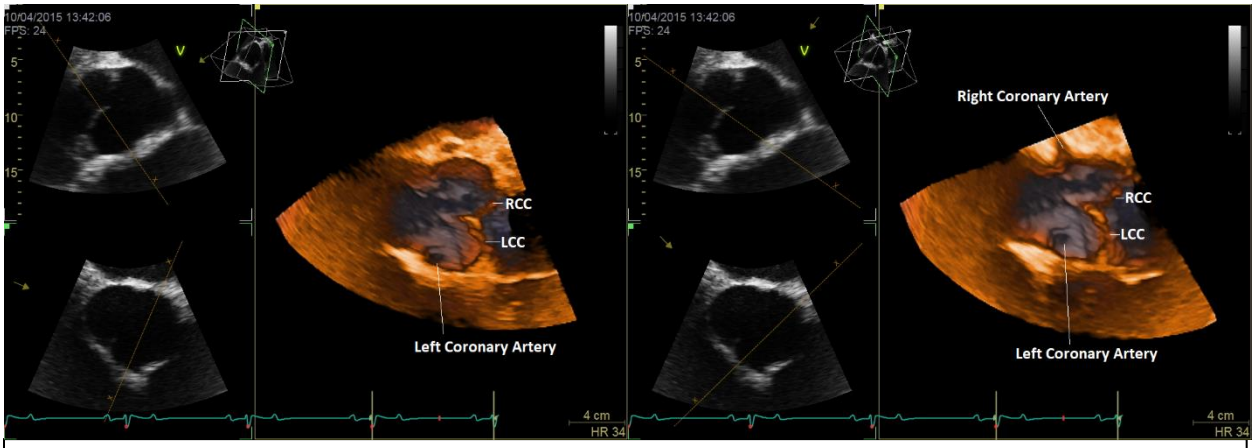

Figure 10: Images from racing Thoroughbred "Ryton." This view is from rotating the enface view left and angling it slightly to visualize the Left and Right Coronary Sinuses. These views are both from the same image, but the right view was rotated slightly from the left and the crop plane adjusted to view a cross section of the Right Coronary Artery. In both views the beginning of the Left Coronary Artery can be seen, appearing as a black circle or hole in the Left Coronary Sinus.

In systole, the enface view of the valve would appear more circular than in diastole. The LCC was often visible adjacent to the walls of the left coronary sinus, while the other two cusps were not (Figure 11). When rotated to the side, with the crop plane between the NCC and RCC and through the center of the LCC, the valve appeared to be relatively cylindrical. The root would have a slightly expanded appearance where the sinuses of Valsalva were, and the LCC could often be seen in its open position from this view as well (Figure 7).

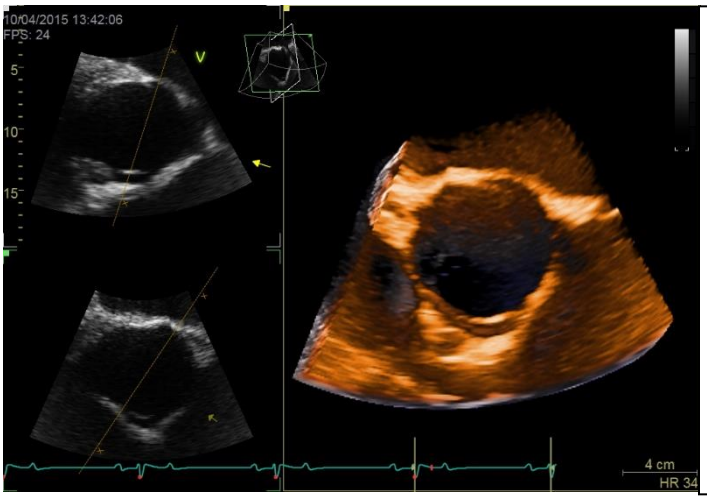

Figure 11: From Thoroughbred "Ryton." The aortic valve is shown from an enface view in systole. While the NCC and RCC cannot be seen in their open positions, the LCC can be seen at the bottom of the valve. The valve overall has a round appearance, rather than the appearance of three circles put together that it has in diastole.

Echocardiographic Anatomy of Aortic Regurgitation Affected Valves from the Right Hemithorax

3DE allows for visualization of abnormal pathology on aortic valves affected by AR. In horses with AR, the valve leaflets themselves tended to be more visible in diastole and have a more opaque appearance throughout. This worsened with the degree of AR. Likewise, the commissures had more visible tissue, especially in affected areas. In some cases, regurgitation of blood could be visualized (Figure 12). In diastole, the NCC and RCC were generally visible along with the LCC from both enface and side views. The more severe the AR, the more visible

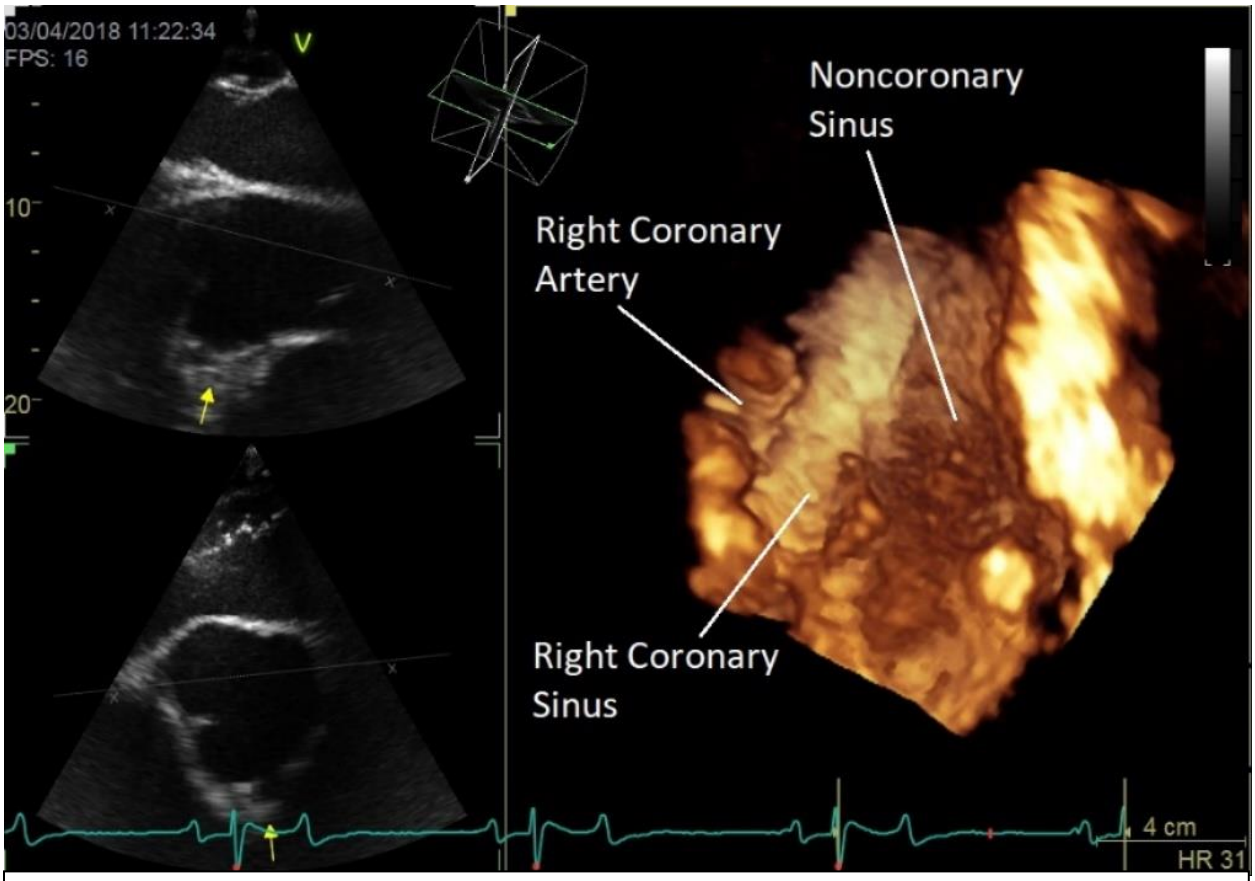

Figure 12: Image from Warmblood "Eric" who had been previously diagnosed with mild AR. This image is from rotating the enface view up, and shows the Right and Noncoronary Sinuses in diastole, as well as a cross-section of the Right Coronary Artery. The dark appearance in the Noncoronary sinus indicates where blood has pooled back into the sinus during diastole. The darker appearance at the bottom of the image, past the Noncoronary sinus, indicates where blood is regurgitating into the left ventricle. The light appearance of the Right Coronary Sinus indicates no blood is regurgitating there, and is what a normal Sinus of Valsalva should look like.

they were (Figure 13). From the side, the valve leaflets had a thickened appearance, again coincident with the level of AR (Figure 13).

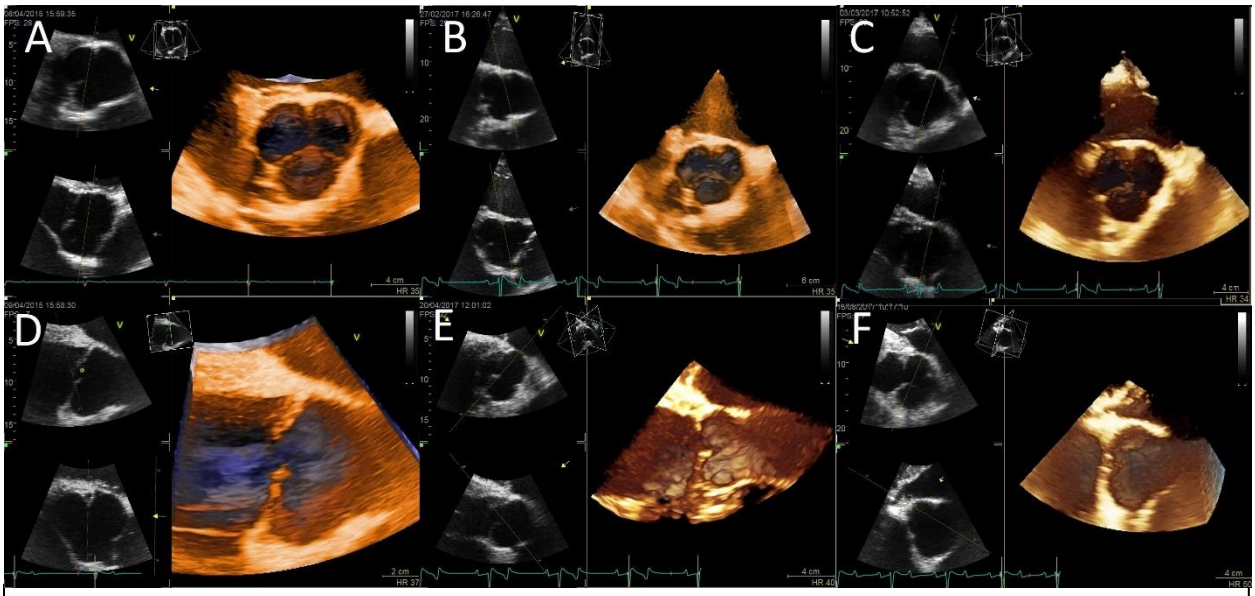

Figure 13: This sequence of images shows the progression from a normal valve (A and D) to mild (B and E) and moderate (C and F) AR. The top images show an enface view of the valve. The commissures and lunulae have a slightly thickened appearance in both B and C, with C appearing thickest. The bottom images show a side view of the valve, and show cross sections of the LCC and NCC. The cusps appear thicker in E than D, and even thicker in F than E. These images are from different horses and are not necessarily representative of disease progression in an individual horse.

It was also possible to visualize a jet lesion in the sinuses of Valsalva in one case. From the front, it appeared similar to an additional lunulae and could be mistaken for a stitch artifact. However, it was present on all follow up examinations and in all images. From a top view, it could be seen as a raised portion of the noncoronary sinus, appearing almost as another interleaflet triangle. It therefore was determined to be a jet lesion (Figure 14).

The only cases of severe AR analyzed were due to endocarditis, and the valve leaflets appeared severely thickened. Two horses with multiple examinations were analyzed; Ari had two examinations, and Sam had three. It was easily visualized which leaflets were affected by the infection. In Ari, all three cusps appeared severely affected. They all appeared almost entirely opaque from an enface view in diastole. In systole, all cusps could be visualized clearly, and the

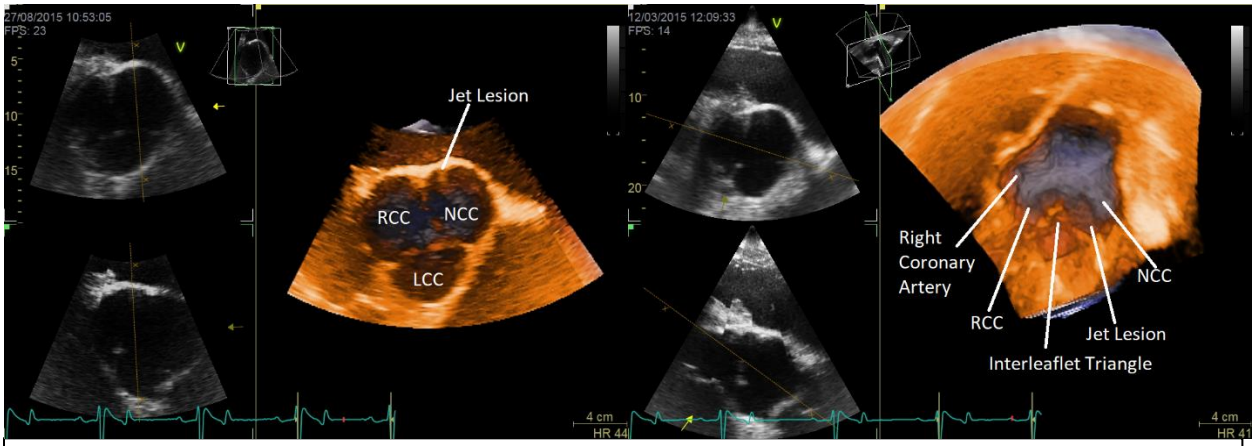

Figure 14: Images from Thoroughbred "Pie" who had been diagnosed with moderate AR. In the enface view to the left, a jet lesion can be seen in the NCC adjacent to the commissure and interleaflet triangle between the NCC and RCC. It appears almost as an additional interleaflet triangle or commissure. In the image to the right, which is a top view of the Right and Noncoronary sinuses, the jet lesion can again be seen within the Noncoronary sinus and looks similar to the interleaflet triangle. While these images were multi-beat, the jet lesion appearance is known to not be a stitch artifact as it was present in all three cardiac examinations of this horse.

size of the valve opening was decreased. From the side, the cusps appeared thickened, and could be visualized clearly in both systole and diastole as well. On Sam's examinations, it was clear that the NCC and RCC were the most affected. The LCC appeared relatively normal from all angles, and was not thickened from the side. However, the commissure between the RCC and NCC from the enface view in diastole had a thick section of visible tissue. From the side, the RCC and NCC were much thicker than the LCC, and were visible in systole (Figure 15).

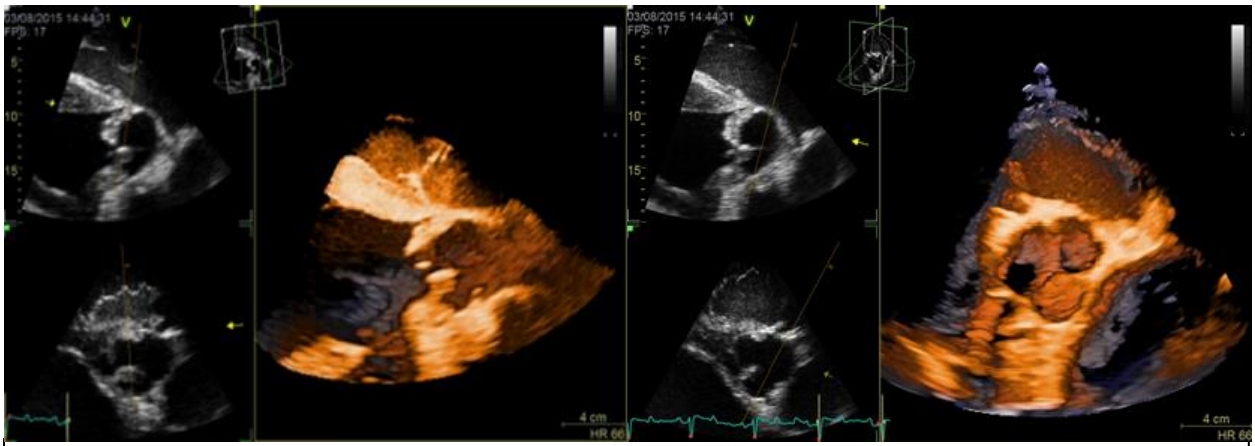

Figure 15: Images from horses with severe AR from endocarditis. The left image is a side view and shows severely thickened LCC and NCC. The opaque appearance throughout the leaflets in the enface view to the right indicates that the cusps are all thickened.

Results from Measurements

Observationally, there appeared to be a consistent range in which both commissural measurements and cusp thickness measurements fell for both normal and the various classifications of AR severity. These measurements were graphed to visually compare average thicknesses by cusp per level of AR, as well as overall average thickness for each level of AR severity. To determine whether there is a statistically significant correlation between any measurements taken and severity of AR, SAS was used for linear regression analysis. All levels of AR were assigned a number score, with 1 being normal, 2 being mild AR, 3 being moderate and 4 being severe in order to compare a predicted AR score with diagnosed AR score. Backwards elimination of variables, in this case the measurements taken, was performed until all remaining measurements were significant with $P \leq 0.15$. This was performed both including and excluding the two severe endocarditis cases, as the endocarditis cases are not indicative of normal disease progression. The variables determined by SAS to be statistically significant when the endocarditis severe AR cases were excluded were the LCC thickness measurement from the side ("LCC"), and the commissural measurement between the NCC and the LCC ("NCCL"). The equation determined the predict AR severity, with an R^2 of 0.7703, is shown below:

$$\text{Predicted AR Score} = -0.44490 + 1.58185(\text{LCC}) + 1.82418(\text{NCCL})$$

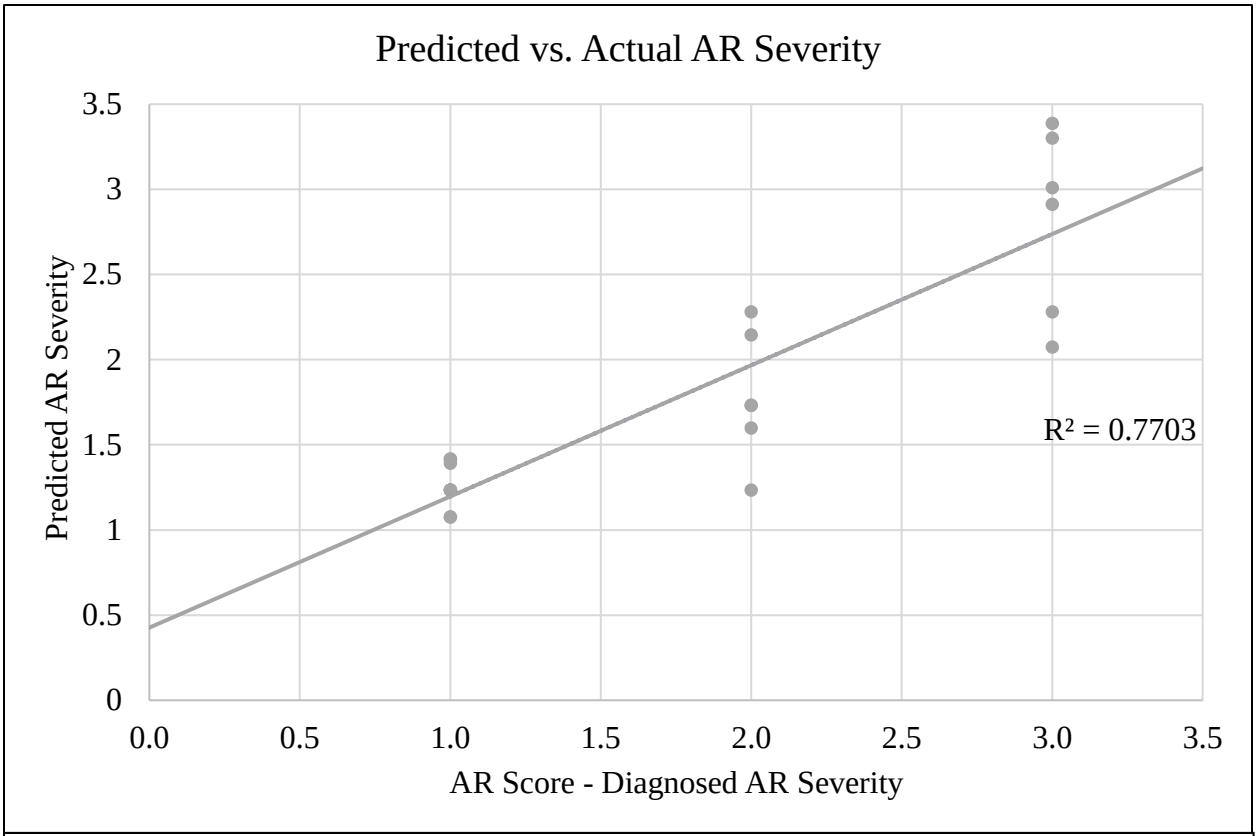

Figure 16: Diagnosed AR severity or "score" plotted against predicted AR severity based on the equation above which did not include data from severe AR cases. The strong linear correlation between predicted score based on valve measurements and actual diagnosed AR severity indicates that the changes to the aortic valve itself are indicative of AR severity and progression.

When the 2 severe AR endocarditis cases were included, SAS determined the significant measurements to be the NCC thickness measurement from the side ("NCC"), commissural measurement between the NCC and LCC ("NCCL"), and the diameter of the valve from a side view in diastole ("DDS"). The equation to predict AR severity with an AR score from these measurements, which had an R^2 of 0.8554, is shown below:

$$\text{Predicted AR Score} = 0.27546 + 2.07319(\text{NCC}) + 2.03489(\text{NCCL}) - 0.14659(\text{DDS})$$

Normal Echocardiographic Anatomy from the Left Hemithorax

Images taken from the left side of the horse were generally of worse quality than those taken from the right. The aortic valve was not visible during the entire cardiac cycle, making it more difficult to visualize during all phases of contraction. It would move out of the echocardiography window for a portion of the cardiac cycle. Still images could be obtained of the valve in diastole from an enface view and edited in EchoPac to appear of reasonable quality. The images often did not appear to show much detail on the Vivid E9, but when color and gain were adjusted in EchoPac images often showed good visualization of at least some parts of the aortic valve, if not the whole thing.

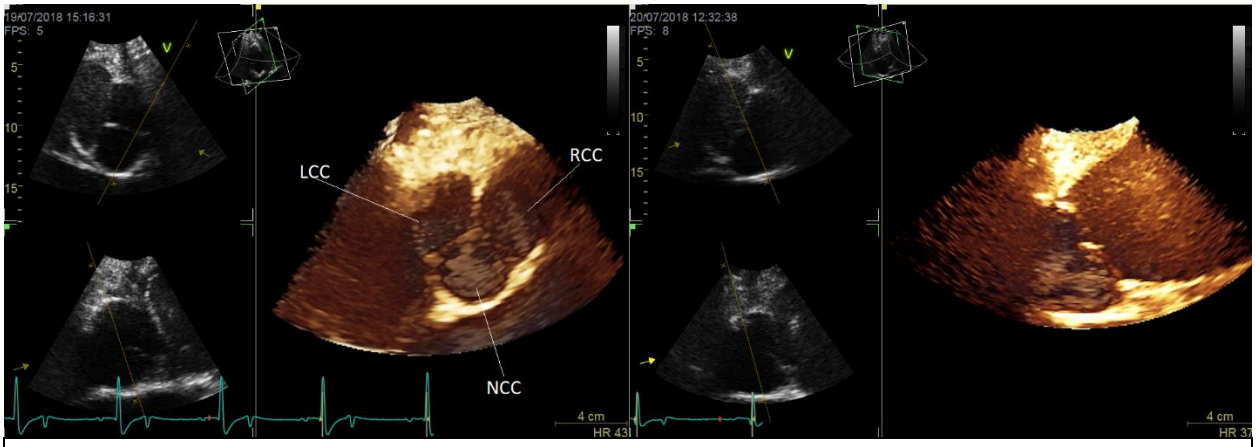

Figure 17: Images of normal aortic valves taken from the left side from racing Thoroughbreds "Dylan" (left) and "Spark" (right). The left image is an enface view, but has an opposite orientation to the standard enface view taken from the right side of the horse. Here, the NCC is at the bottom and furthest from the transducer, while the LCC is top left and RCC is top right. The NCC is the clearest, with greatest visualization of the NCC itself as well as the borders of the noncoronary sinus. The RCC is slightly better visualized than the LCC, with more tissue showing throughout the cusp. However, there the borders of the left coronary sinus can be better visualized than the right coronary sinus. The image to the right shows a side view of the aortic valve, displaying cross sections of the NCC and LCC. The cusps appear thin and noncontinuous, similar to the corresponding view of an image taken from the right side.

In left-sided still enface images in diastole, the cusp at the bottom of the screen furthest from the transducer was always the NCC, while the RCC would be top right and LCC would be top left (Figure 17). Similar to how the LCC was most well defined in right-sided images and

also at the bottom of the screen, the NCC was generally most well defined in left-sided images. In some images the RCC was also well defined, but the LCC was rarely defined. The tissue throughout the NCC was more well defined, and in some better-quality images the same was true of the other cusps. This could provide a way to see defects in the valve leaflets themselves, if good quality images can be obtained.

In general, the left-sided images appeared grainier and less defined that right-sided images of the aortic valve. Side view images in diastole showed cross sections of the cusps, but the tissue was not always visible throughout (Figure 17). Views of the sinuses of Valsalva could be obtained, but were generally of worse quality than from right-sided images. In most images, the wall of the left coronary sinus was not defined in the image. Therefore, cross-sectional views of the right coronary artery could be obtained, but rarely the same was true of the left coronary artery (Figure 18). However, the noncoronary sinus could be visualized in great detail.

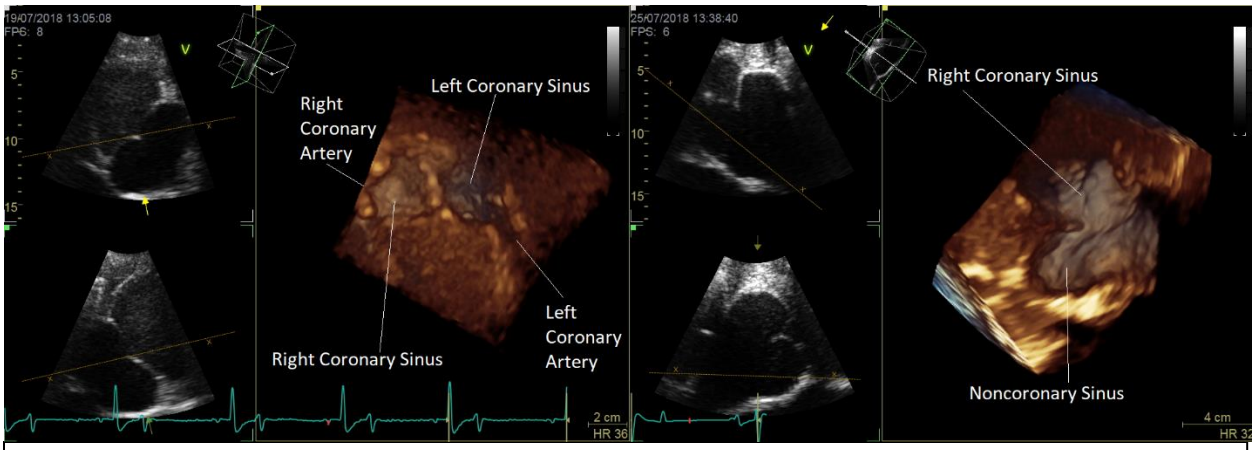

Figure 18: Two top views of the Sinuses of Valsalva from left-sided images from racing Thoroughbreds "Diamond" (left) and "Ryalex" (right). The left image shows the Right and Left Coronary Sinuses, along with cross sections of both coronary arteries. Only the mouth of the Right Coronary Artery is visible, but it is clearly the opening to an artery and the walls of the sinus form a "V" leading towards it. A longer cross section of the Left Coronary Artery is visible, but in less detail than the right. The right image shows the Right and Noncoronary Sinuses. No Coronary arteries are visible from this angle. The Noncoronary sinus can be visualized in great detail, with clear borders to the sinus whereas there are not clear edges of the Right Coronary Sinus.

Discussion

3DE allows for better visualization of the aortic valve than standard echocardiographic methods, as more minute anatomical structures can be seen from manipulation of the 3D images. These include the Sinuses of Valsalva, Coronary Arteries, Interleaflet Triangles, and the 3 cusps. 3DE is also less dependent on the angle of the transducer for accurate imaging of valve structures and indications of regurgitation, so therefore is a more accurate diagnostic method (Chien-Chia Wu & Takeuchi, 2017). It has also been shown to take more accurate aortic valve measurements than 2D when compared to left heart catheterization with aortography and surgical measurements (Fang, et al., 2005). Additionally, 3DE is better for determining the orientation of the aortic valve and therefore identification of the cusps and related structures. On 2D, it can be difficult to tell whether a short axis view is looking from the back or front of the valve, i.e. from the aorta or the left ventricle, as a 2D image is a tomographic slice through the valve. A true enface view should be looking at the valve from the aorta, but when the short axis view is a close-up on the valve, and it is impossible to rely on the location of other structures in the heart in relation to the aorta, it can be difficult to determine from which direction the valve is being imaged. This is especially true when looking at previously taken images. On 3DE, there is more freedom to manipulate previously taken images and determine location of anatomical structures within the valve. One image can be manipulated to find the coronary arteries, from which it can be determined which cusp is which. It is also possible to tell which side of the valve faces the aorta and which faces the left ventricle in one previously taken image. This allows for more accurate analysis of images, as the clinician can be sure which areas of the valve are affected by any potential issues.

Anecdotally, it has been noted that the cusps in the aortic valve thicken when AR is present (Reef & Spencer, 1987). However, no absolute quantifiable measure of this exists, which

this study attempted to rectify. All valve measurements in this study were novel and not based on any previous study's indications of significance. As such, not all measurements were necessarily significant to the severity of AR in the horse. There was also no standard breed used; while all normal images analyzed were from Thoroughbreds, the same was not true of abnormal valves imaged. Horses affected by AR included in this study ranged from Exmoor ponies to Warmbloods. Warmbloods would have larger hearts than ponies, as they are much larger animals, so it is likely the valve measurements are not necessarily comparable. Al-Haider, et al. (2017) looked at 2D echocardiographic measurements in various horses breeds, including ponies, with the aim of finding reference values for each breed studied based on body size. One measurement taken was aortic internal diameter, which varied by breed and was shown to be larger in larger breeds such as Warmbloods, Drafts and Thoroughbreds and smaller in Ponies (Al-Haider, et al., 2017). The valve diameter and circumference measurements showed great variability by breed and showed no correlation to AR presence or severity. However, aortic valve diameter measurements on the normal Thoroughbred horses taken in this study were within the same range as standard measurements taken on normal Thoroughbreds in both M-mode and 2D in another study (Patteson, Gibbs, Wotton, & Cripps, 1995). This indicates that while this measurement may not be of use in AR diagnostics, it is at least relatively accurate.

The cusp thickness measurements, namely the commissural measurements and the thicknesses of the cusps from a side view, stayed fairly consistent within each level of AR severity across all breeds. Statistical analysis mostly supported this observation. When the severe AR cases were included, SAS determined the significant measurements to be the NCC thickness from the side, the thickness of the commissure between the NCC and the LCC, and the diameter of the valve from the side in diastole. While this corresponding equation had an R^2 of 0.8554, it

is not necessarily accurate as the two severe cases were from endocarditis. One endocarditis case, a horse named Sam, had a severely thickened NCC as this was where the majority of the infection had settled. This likely skewed the data and could be the reason that the NCC was the cusp of most significance in this statistical analysis. Additionally, the diameter of the valve in diastole was negatively correlated to AR severity in this equation, which may have been due to the thickening of the cusps from endocarditis making the diameter of the valve itself smaller in the severe cases. When the endocarditis cases were excluded, SAS determined the significant measurements to be the thickness of the LCC from the side, and the commissure between the NCC and LCC. The R^2 for the corresponding equation was 0.7703; lower than the other equation, but still a strong linear correlation. This equation is also likely more accurate, as it is not skewed by severe thickening from an infection. Both significant measurements were including the LCC, which supports the findings by Reef and Spencer that the LCC was the cusp most affected by thickening due to AR (Reef & Spencer, 1987).

When the aortic valve was imaged from the left, the valve was more difficult to find with the probe, as the left lung is larger and between the probe and the aortic valve from the left. Likewise, the cardiac window is smaller from the left. While the aortic valve is part of the left side of the heart, its orientation actually falls slightly to the right side of the heart, and the cardiac window is better due to less lung being in the way. Therefore, the aortic valve is more easily visualized with echocardiography from the right (Long, Bonagura, & Darke, 1992). The images from the left were generally much grainer in appearance and of lower resolution than images taken from the right, and they took more manipulation in EchoPac to visualize structures in the valve. Likewise, while some good still images could be obtained, especially in diastole, the moving images of the cardiac cycle were not as usable as the ones from the right as the heart

would move out of the imaging window throughout the cycle from the left. The one advantage to left sided images is that the NCC and RCC were the most clearly visualized when images were of good quality, as opposed to the LCC being most clearly visualized from the right. Therefore, there is potential for left-sided images to be of use in locating defects of the aortic valve. Lastly, when images were of good quality more of the tissue throughout the cusps was able to be visualized in diastole from an enface view, as opposed to right-sided images where the cusps in normal valves appeared mostly black throughout. This may be because there is less depth to the image, as the left side of the heart is closer to the left side of the horse and therefore the probe in this case. Again, there is the potential for left-sided images to be of use in locating defects in the center of cusps.

It should be noted that most images in this study were from Thoroughbreds (all normal horses and 8 horses with AR), which are generally of a slimmer build than other breeds, especially heavier breeds like Warmbloods and Draft breeds. Slimmer horses have more potential for obtaining good quality echocardiograms, as the thorax is less deep and there is less fat between the transducer and the heart. Cardiac evaluation is extremely dependent on image quality, especially in the case of the images of the aortic valve taken from the left side of the horse. While there may be potential for these novel views to be of use diagnostically, it is unlikely that this would be true in all cases as good images are difficult to obtain. This is true of both 2D and 3D images from the left, as it has to do with imaging window quality and not the imaging technology itself. All left-sided images in this study were from thin racing Thoroughbreds, and many of the images obtained were still not of adequate quality for cardiac evaluation.

In humans, it is recommended by the European Association of Cardiovascular Imaging that the 2D transthoracic echocardiography (TTE) be followed by 2D transesophageal echocardiography (TOE) when TTE is insufficient of when further diagnostics are required (Lancelotti, et al., 2013). TOE allows for more accurate imaging of the heart, as it allows the probe to get closer to the heart for clearer images. However, this is not possible in horses currently due to the length of the horse's neck and long enough probes not being commercially available. Producing one long enough for a horse would be expensive, and not necessarily cost effective as it could be easily destroyed by the horse. While it has been done, it has only been done experimentally. Young et al. (1996) looked at TOE as a method to evaluate cardiac output in anesthetized horses and found it to be an effective method. However, this was more than 20 years ago and has not become a relevant method in veterinary practice.

For horses, 3DE provides a good secondary method of cardiac evaluation. Even in humans it can provide additional diagnostic potential, especially with complex lesions, as it provides a comprehensive look at the valve to allow for more accurate quantification of hemodynamic consequences of regurgitation on chambers of the heart (Lancelotti, et al., 2013). Human medicine also has the ability to use Cardiac Magnetic Resonance Imaging (CMRI), which is not a possibility in horses as machines large enough to fit an equine thorax do not exist. CMRI is the gold standard for assessment of LV volumes and ejection fraction in humans (Everett, Newby, Jabbour, Fayad, & Dweck, 2016). These measurements are useful in AR diagnosis, as AR causes changes to the LV. Since CMRI is not available in equine medicine, 3DE is the best available technology for cardiac evaluation and diagnosis of AR severity, as it allows for the imaging of 3D sections of tissue, as does MRI.

References

Al-Haider, A., Moula, N., Leroux, A., Farnir, F., Deleuze, S., Sanderson, C., & Amory, H. (2017). Reference values of two-dimensional and M-mode echocardiographic measurements as a function of body size in various equine breeds and in ponies. *Journal of Veterinary Cardiology*, 492-501.

Anderson, R. (2000). Clinical Anatomy of the Aortic Root. *Heart, 84*(6), 670-673. doi:10.1136/heart.84.6.670

Baumgartner, H., Hung, J., Bermejo, J., Chambers, J. B., Edvardsen, T., Goldstein, S., . . . Otto, C. (2017). Recommendations on the echocardiographic assessment of aortic valve stenosis: a focused update from the european association of cardiovascular imaging and the American Society of Echocardiography. *European Heart Journal, 18*, 254-275. doi:10.1093/ehjci/jew335

Borer, J. S. (2016). Aortic Valve Surgery for Aortic Regurgitation. *Journal of the American College of Cardiology, 68*(20), 2154-2157. doi:10.1016/j.jacc.2016.09.003

Chambers, J. B., Myerson, S. G., Rajani, R., Morgan-Hughes, G. J., & Dweck, M. R. (2016). Multimodality imaging in heart valve disease. *Open Heart, 3*, 1-7. doi:10.1136/openhrt-2015-000330

Chien-Chia Wu, V., & Takeuchi, M. (2017). Three-Dimensional Echocardiography: Current Status and Real-Life Applications. *Acta Cardiologica Sinica, 33*(2), 107-118. doi:10.6515/ACS20160818A

Else, R. W., & Holmes, J. R. (1972). Cardiac Pathology in the Horse (2) Microscopic Pathology. *Equine Veterinary Journal, 4*(2), 57-63. doi:10.1111/j.2042-3306.1972.tb03879.x

Else, R., & Holmes, J. (1972). Cardiac Pathology in the Horse (1) Gross Pathology. *Equine Veterinary Journal, 4*(1), 1-8. doi:10.1111/j.2042-3306.1972.tb03868.x

Everett, R., Newby, D., Jabbour, A., Fayad, Z., & Dweck, M. (2016). The Role of Imaging in Aortic Valve Disease. *Current Cardiovascular Imaging Reports, 9*(21). doi:10.1007/s12410-016-9383-z

Fang, L., Hsiung, M. C., Miller, A. P., Nanda, N. C., Yin, W. H., Young, M. S., & Velayudhan, D. E. (2005). Assessment of Aortic Regurgitation by Live Three-Dimensional Transthoracic Echocardiographic Measurements of Vena Contracta Area: Usefulness and Validation. *Echocardiography, 22*(9), 775-782.

Flachskampf, F. A., Badano, L., Daniel, W., Feneck, R., Fox, K., Fraser, A. G., . . . Zamorano, J. (2010). Recommendations for transoesophageal echocardiography: update 2010. *European Journal of Echocardiography, 11*, 557-576. doi:10.1093/ejechocard/jeq057

Gazi, M., Makhdoomi, D., Abbas, H., Parrah, J., Ganai, A., Dar, S., & Moulvi, B. (2015). Advances of Echocardiography in Equine Practices - A Review. *Journal of Veterinary Science & Technology, 06*(03). doi:10.4172/2157-7579.1000228

Gill, H., & Hoffman, A. (2010). The Timing of Onset of Mechanical Systole and Diastole in Reference to the QRS-T Complex: a Study to Determine Performance Criteria for a Non-Invasive Diastolic Timed Vibration Massage System in Treatment of Potentially Unstable Cardiac Disorders. *Cardiovascular Engineering, 10*, 235-245. doi:10.1007/s10558-010-9108-x

Hallowell, G., & Bowen, M. (2013). Reliability and Identification of Aortic Valve Prolapse in the Horse. *BMC Veterinary Research, 9*(1), 9. doi:10.1186/1746-6148-9-9

Ho, S. Y. (2009). Structure and anatomy of the aortic root. *European Journal of Echocardiography, 10*, 3-10. doi:10.1093/ejechocard/jen243

Holmes, J., & Else, R. (1972). Cardiac Pathology in the Horse (3) Clinical Correlations. *Equine Veterinary Journal, 4*(4), 195-204. doi:10.1111/j.2042-3306.1972.tb03908.x

Jago, R., & Keen, J. (2017). Identification of Common Equine Cardiac Murmurs. *In Practice, 39*, 222-232. doi:10.1136/inp.j1769

Keen, J. (2016). Equine Aortic Regurgitation: The Search for Objective Repeatable and Reproducible Indicators of Severity. *The Veterinary Journal, 213*, 91-92. doi:10.1016/j.tvjl.2016.04.016

Lancelotti, P., Tribouilloy, C., Hagendorff, A., Popesca, B., Edvardsen, T., Pierard, L., . . . Zamorano, J. (2013). Recommendations for the Echocardiographic Assessment of Native Valvular Regurgitation: an Executive Summary from the European Association of Cardiovascular Imaging. *European Heart Journal - Cardiovascular Imaging, 14*(7), 611-644. doi:10.1093/ehjci/jet105

Lang, R., Badano, L., Tsang, W., Adams, D., Agricola, E., Buck, T., . . . Zoghbi, W. (2012). EAE/ASE Recommendations for Image Acquisition and Display Using Three-Dimensional Echocardiography. *Journal of the American Society of Echocardiography, 25*(1), 3-46. doi:10.1016/j.echo.2011.11.010

Long, K. J., Bonagura, J., & Darke, P. (1992). Standardised imaging technique for guided M-mode and Doppler echocardiography in the horse. *Equine Veterinary Journal, 24*(3), 226-235. doi:10.1111/j.2042-3306.1992.tb02820.x

Marr, C. (2016). Cardiac and Respiratory Disease in Aged Horses. *Veterinary Clinics of North America: Equine Practice, 32*(2), 283-300. doi:10.1016/j.cveq.2016.04.006

Marr, C., & Bowen, I. (2010). *Cardiology of the Horse.* Edinburgh: Saunders/Elsevier.

Muraru, D., Badano, L. P., Vannan, M., & Iliceto, S. (2012). Assessment of aortic valve complex by three-dimensional echocardiography: a framework for its effective application in clinical practice. *European Heart Journal, 13*, 541-555. doi:10.1093/ehjci/jes075

Nishimura, R. A., Otto, C. M., Bonow, R. O., Carabello, B. A., Erwin, J. P., Guyton, R. A., . . . Thomas, J. D. (2014). 2014 AHA/ACC Guideline for the Management of Patients with Valvular Heart Disease. *Journal of the American College of Cardiology, 63*(22), 57-156. doi:10.1016/j.jacc.2014.02.536

Nishimura, R. A., Otto, C. M., Bonow, R., Carabello, B. A., Erwin, J. P., Fleisher, L. A., . . . Thompson, A. (2017). 2017 AHA/ACC Focused Update of the 2014 AHA/ACC Guideline for the Management of Patients with Valvular Heart Disease. *Journal of the American College of Cardiology, 70*(2), 252-289. doi:10.1016/jacc.2017.03.011

Orton, E. C. (2013). Valvular Heart Disease. *Small Animal Soft Tissue Surgery, 1*, 807-814.

Patteson, M., Gibbs, C., Wotton, P., & Cripps, P. (1995). Echocardiographic measurements of cardiac dimensions and indices of cardiac function in normal adult Thoroughbred horses. *Equine Veterinary Journal, 19*, 18-27.

Rageer, M. V., Versteegh, M. I., Klautz, R. J., Stijnen, T., Schalij, M. J., Bax, J. J., . . . Delgado, V. (2015). Aortic Valve Repair Versus Replacement for Aortic Regurgitation: Effects on Left Ventricular Remodeling. *Journal of Cardiac Surgery*, 13-19.

Reef, V., & Spencer, P. (1987). Echocardiographic Evaluation of Equine Aortic Insufficiency. *American Journal of Veterinary Research, 48*(6), 904-909.

Reef, V., Bonagura, J., Buhl, R., McGurrin, M., Schwarzwald, C., Van Loon, G., & Young, L. (2014). Recommendations for Management of Equine Athletes with Cardiovascular Abnormalities. *Journal of Veterinary Internal Medicine, 28*(3), 749-761. doi:10.1111/jvim.12340

Seo, Y., Ishizu, T., & Aonuma, K. (2014). Current Status of 3-Dimensional Speckle Tracking Echocardiography: A Review from Our Experiences. *Journal of Cardiovascular Ultrasound, 22*(2), 49-57. doi:10.4250/jcu.2014.22.2.49

Stugaard, M., Koriyama, H., Katsuki, K., Masuda, K., Asanuma, T., Takeda, Y., . . . Nakatani, S. (2015). Energy loss in the left ventricle obtained by vector flow mapping as a new quantitative measure of severity of aortic regurgitation: a combined experimental and clinical study. *European Heart Journal, 16*, 723-730. doi:10.1093/ehjci/jev035

Sutton, J., Ho, S., & Anderson, R. (1995). The Forgotten Interleaflet Triangles: A Review of the Surgical Anatomy of the Aortic Valve. *The Annals of Thoracic Surgery, 59*(2), 419-427. doi:10.1016/0003-4975(94)00893-c

Ven, S., Decloedt, A., Van Der Vekens, N., De Clercq, D., & Van Loon, G. (2016). Assessing Aortic Regurgitation Severity from 2D, M-Mode and Pulsed Wave Doppler Echocardiographic Measurements in Horses. *The Veterinary Journal, 210*, 34-38. doi:10.1016/j.tvjl.2016.01.011

Young, L. (2007). Equine Aortic Valve Regurgitation: A Disease Worthy of Further Consideration. *Equine Veterinary Education, 19*(9), 469-470. doi:10.2746/095777307x238552

Young, L., Blissitt, K., Bartram, D., Clutton, R., Molony, V., & Jones, R. (1996). Measurement of Cardiac Output by Transoesophageal Doppler Echocardiography in Anaesthetized Horses: Comparison with Thermodilution. *British Journal of Anaesthesia*, *77*, 773-780.

Appendix

Abbreviation Key:

AV	Aortic Valve
LCC	Left Coronary Cusp
RCC	Right Coronary Cusp
NCC	Noncoronary Cusp
LV	Left Ventricle
LVOT	Left-Ventricular Outflow Tract
AR	Aortic Regurgitation
AF	Atrial Fibrillation
VSD	Ventricular Septal Defect
2D	Two-Dimensional
3DE	Three-Dimensional Echocardiography
TTE	Transthoracic Echocardiography
TOE	Transesophageal Echocardiography
CMRI	Cardiac Magnetic Resonance Imaging

Normal Measurements:

All measurements made in EchoPac on normal aortic valves in cm or cm^2.

Name	Image Number	FPS	Commisural Measurement			Sino-tubular junction Area					
						Systole			Diastole		
			RCC/NCC	NCC/LCC	LCC/RCC	1	2	3	1	2	3
Mac	12	6	0.4	0.4	0.4	39.7	39.0	39.7	51.1	49.9	50.6
Ryton	12	24	0.5	0.4	0.4	56.1	53.6	54.1	50.0	51.7	50.7
Bescot	11	7	0.4	0.4	0.4	42.9	47.2	47.6	46.5	49.7	46.5
Joe	11	19	0.5	0.5	0.5	47.5	47.9	47.2	56.0	53.1	56.5
Ultra	10	7	0.5	0.4	0.4	57.0	56.5	56.7	57.9	57.4	57.8
Ballycool	12	25	0.5	0.5	0.5	62.1	57.6	58.7	54.6	56.2	53.4
Ben	10	28	0.4	0.4	0.4	53.7	53.1	54.8	55.5	55.1	56.3
Morning	13	6	0.5	0.4	0.4	44.9	46.4	43.4	52.1	53.3	51.8
Thorpe	12	11	0.4	0.4	0.4	38.3	40.3	42.0	38.9	40.0	42.6

Name	Valve diameter Systole						Valve diameter Diastole						Cusp Thickness		
	Front			Side			Front			Side			Side		
	1	2	3	1	2	3	1	2	3	1	2	3	LCC	RCC	NCC
Mac	6.9	7.4	6.7	8.1	8.5	8.5	7.5	8.1	7.4	7.7	7.7	7.8	0.6	0.6	0.6
Ryton	8.0	8.6	8.7	6.5	6.4	6.4	7.8	7.7	7.1	7.4	7.4	7.1	0.5	0.5	0.5
Bescot	7.5	7.2	8.2	7.2	7.2	7.3	7.1	7.8	7.7	6.4	6.4	6.4	0.5	0.5	0.5
Joe	7.9	7.4	7.6	7.7	8.0	7.8	7.3	8.4	8.4	8.2	8.3	8.1	0.6	0.7	0.6
Ultra	7.7	8.9	8.9	7.3	7.3	7.2	8.1	8.3	8.4	8.1	8.2	8.2	0.7	0.7	0.7
Ballycool	8.3	9.0	8.4	7.2	7.3	7.1	7.6	8.0	8.4	7.3	7.4	7.5	0.6	0.6	0.6
Ben	8.0	8.2	8.2	7.4	7.6	7.8	8.6	7.7	8.3	7.6	7.6	7.2	0.6	0.6	0.6
Morning	7.2	7.5	8.0	8.1	8.3	8.7	7.3	8.4	7.8	8.3	8.1	8.0	0.6	0.6	0.6
Thorpe	7.2	7.3	7.4	6.3	6.3	6.6	6.6	7.0	7.3	5.9	5.9	6.4	0.6	0.6	0.6

Average Normal Measurements:

The averaged values of measurements taken on normal valves, in cm or cm^2.

Name	Image Number	FPS	Commisural Measurement			Valve Area (Avg)		Circumference (Avg)		Diameter Systole (Avg)		Diameter Diastole		Cusp Thickness Side		
			RCC/NCC	NCC/LCC	LCC/RCC	Systole	Diastole	Systole	Diastole	Front	Side	Front	Side	LCC	RCC	NCC
Mac	12	6	0.4	0.4	0.4	39.47	50.53	22.77	26.40	7.00	8.37	7.67	7.73	0.6	0.6	0.6
Ryton	12	24	0.5	0.4	0.4	54.60	50.80	27.13	26.60	8.43	6.43	7.53	7.30	0.5	0.5	0.5
Bescot	11	7	0.4	0.4	0.4	45.90	47.57	24.80	25.67	7.63	7.23	7.53	6.40	0.5	0.5	0.5
Joe	11	19	0.5	0.5	0.5	47.53	55.20	24.80	27.37	7.63	7.83	8.03	8.20	0.6	0.7	0.6
Ultra	11	27	0.5	0.4	0.4	56.73	57.70	27.50	28.20	8.50	7.27	8.27	8.17	0.7	0.7	0.7
Ballycool	12	25	0.5	0.5	0.5	59.47	54.73	28.10	27.17	8.57	7.20	8.00	7.40	0.6	0.6	0.6
Ben	10	28	0.4	0.4	0.4	53.87	55.63	26.97	27.77	8.13	7.60	8.20	7.47	0.6	0.6	0.6
Morning	13	6	0.5	0.4	0.4	44.90	52.40	24.40	26.63	7.57	8.37	7.83	8.13	0.6	0.6	0.6
Thorpe	12	11	0.4	0.4	0.4	40.20	40.50	23.03	23.90	7.30	6.40	6.97	6.07	0.6	0.6	0.6
Average			0.46	0.42	0.42	49.19	51.67	25.50	26.63	7.86	7.41	7.78	7.43	0.59	0.60	0.59
Standard Deviation			0.05	0.04	0.04	6.95	5.03	1.90	1.24	0.62	0.69	0.52	0.73	0.06	0.07	0.06
Min			0.4	0.4	0.4	38.3	38.9	22.4	23.4	6.7	6.3	6.6	5.9	0.5	0.5	0.5
Max			0.5	0.5	0.5	62.1	57.9	28.7	28.4	9.0	8.7	8.6	8.3	0.7	0.7	0.7

Disease Measurements:

All measurements made in EchoPac on aortic valves affected by aortic regurgitation of varying degrees, in cm or cm^2.

Diagnosis	Name	Last Name	Breed	Date	Image #	FPS	Commisural Measurement			Valve Area					
							RCC/NCC	NCC/LCC	LCC/RCC	Systole			Diastole		
										1	2	3	1	2	3
AV Endocarditis	Sam	Gleneagles		2/4/2018	34	13	1.8	0.4	0.4	61.9	61.6	62.6	59.0	58.4	58.5
	Ari	Exmoor Trekk	Exmoor Pony	6/7/2015	32	31	1.0	0.5	0.5	31.7	32.1	32.0	26.2	26.4	27.9
Mild AR	Eric	Meldrum	Warmblood	3/4/2018	34	16	0.4	0.9	0.4	50.8	50.9	50.5	43.4	47.7	43.4
	Rosie	Crisp	TB	20/09/2017	33	6	0.4	0.6	0.6	58.6	59.7	57.6	57.9	58.1	58.4
	Sprite	Szczuka		20/04/2017	22	22	0.4	0.5	0.4	31.4	31.4	30.8	24.4	26.5	25.9
	Rudi	Finch	TB	27/02/2017	20	29	0.4	0.4	0.4	61.7	64.2	68.2	57.9	52.3	55.0
	Lexi	Munro	TBX	8/1/2016	17	18	0.5	0.8	0.5	52.6	51.6	51.9	50.0	51.7	48.5
	Tiny	Stenhouse		10/9/2015	20	15	0.6	0.5	0.5	58.9	54.8	54.9	55.2	52.8	55.8
Moderate AR	Lordy	McGarry	TBX	16/08/2017	35	21	1.0	0.8	0.8	54.8	58.4	64.5	63.1	59.1	60.7
	Rudi	Barton	Warmblood	3/3/2017	34/35	23	1.7	0.8	0.8	62.3	61.2	60.2	58.9	59.1	56.6
	Rosie	Thompson	Irish Sp H	16/11/2016	43	16	1.0	0.6	0.6	59.1	61.2	56.5	57.4	60.9	57.9
	Pie	Baird	TB	25/07/2014	24	12	0.7	1.2	0.7	79.4	76.1	79.9	72.3	71.1	72.4
	Bessie	Fraser	TB	16/09/2015	17	14	1.0	1.1	0.6	69.8	69.5	70.4	64.4	65.8	64.3
	Hugo	McNaughton	hunter	29/06/2016	30	40	0.5	0.8	0.5	59.3	62.2	62.2	76.0	70.9	72.6

Name	Valve Circumference						Valve diameter Systole						Valve diameter Diastole						Cusp Thickness		
	Systole			Diastole			Front			Side			Front			Side			Side		
	1	2	3	1	2	3	1	2	3	1	2	3	1	2	3	1	2	3	LCC	RCC	NCC
Sam	28.5	28.5	28.9	28.2	28.5	28.5	9.1	8.8	9.0	8.8	8.9	9.0	8.5	8.5	8.4	8.6	8.9	9.2	0.6	2.3	2.1
Ari	20.3	20.5	20.5	19.0	19.4	19.6	6.3	6.5	6.2	5.1	5.4	5.8	5.3	5.8	6.1	4.7	4.7	4.8	0.9	1.4	1.5
Eric	25.9	26.3	26.0	24.2	25.4	24.1	7.7	8.0	8.2	8.0	8.2	7.9	7.7	7.7	7.8	8.4	9.0	9.0	0.6	0.7	0.7
Rosie	27.8	28.5	28.1	28.1	28.5	28.6	8.9	8.0	9.6	8.1	8.3	8.4	8.4	8.7	8.3	9.1	9.4	9.1	0.6	0.6	0.6
Sprite	20.5	20.2	20.0	18.2	19.1	18.8	6.1	6.5	6.3	6.0	6.1	6.1	5.4	5.5	6.0	6.2	6.2	6.2	0.8	0.6	0.6
Rudi	28.5	29.1	30.0	28.2	27.0	27.6	8.7	9.6	8.5	7.5	7.5	8.2	7.7	8.2	8.3	8.0	8.1	8.1	0.6	0.6	0.6
Lexi	27.9	26.4	26.8	26.6	26.5	25.6	8.1	8.7	8.3	8.0	7.9	8.2	7.7	7.4	7.6	6.9	7.0	7.0	0.8	0.6	0.6
Tiny	27.9	27.0	26.9	27.5	27.1	27.7	8.2	8.4	8.9	8.6	8.5	8.7	8.2	8.2	7.3	7.8	7.8	7.8	0.8	0.7	0.8
Lordy	26.8	27.9	29.3	29.1	28.6	29.5	8.1	8.2	8.9	9.4	9.5	9.5	8.2	8.4	9.4	9.3	9.4	9.2	1.5	0.8	1.3
Rudi	28.4	28.3	28.0	27.8	28.4	27.7	9.0	8.8	8.9	9.2	9.0	9.3	8.6	8.4	8.7	8.9	9.0	8.9	1.2	1.3	1.3
Rosie	27.7	28.3	27.0	27.6	28.6	27.8	8.4	8.6	8.9	8.0	8.2	8.3	8.7	8.8	8.9	6.9	7.5	7.3	0.9	0.7	0.9
Pie	32.5	31.9	32.8	31.3	31.2	31.1	9.6	10.1	10.1	9.8	9.8	9.8	9.1	9.0	9.4	8.2	8.3	8.3	0.8	0.8	0.7
Bessie	30.4	30.4	30.3	29.6	30.4	29.8	9.6	8.7	9.7	8.8	8.9	8.8	9.3	8.7	8.7	9.1	9.3	9.4	1.1	0.7	1.0
Hugo	27.9	28.3	28.6	32.1	31.9	31.7	8.2	9.6	8.6	8.7	8.4	8.5	8.9	9.5	10.2	8.7	8.7	8.7	0.8	0.7	0.9

Average Diseased Valve Measurements:

The averaged values of measurements taken on aortic valves affected by aortic regurgitation to varying degrees, in cm or cm^2.

Diagnosis	Name	Last Name	Breed	Date	Image #	FPS	Commisural Measurement			Valve Area		Circumference		Diameter				Cusp Thickness		
														Systole		Diastole		Side		
							RCC/NCC	NCC/LCC	LCC/RCC	S	D	S	D	Front	Side	Front	Side	LCC	RCC	NCC
	Sam	Gleneagles		2/4/2018	34	13	1.8	0.4	0.4	62.03	58.63	28.63	28.40	8.97	8.90	8.47	8.90	0.6	2.3	2.1
	Ari	Exmoor Trekk	Exmoor Pony	6/7/2015	32	31	1	0.5	0.5	31.93	26.83	20.43	19.33	6.33	5.43	5.73	4.73	0.9	1.4	1.5
						Average	1.40	0.45	0.45	46.98	42.73	24.53	23.87	7.65	7.17	7.10	6.82	0.75	1.85	1.80
						Standard Deviation	0.40	0.05	0.05	15.05	15.91	4.10	4.54	1.32	1.75	1.39	2.09	0.15	0.45	0.30
						Min	1.00	0.40	0.40	31.70	26.20	20.30	19.00	6.20	5.10	5.30	4.70	0.60	1.40	1.50
						Max	1.80	0.50	0.50	62.60	59.00	28.90	28.50	9.10	9.00	8.50	9.20	0.90	2.30	2.10
Mild AR	Eric	Meldrum	Warmblood	3/4/2018	34	16	0.4	0.9	0.4	50.73	44.83	26.07	24.57	7.97	8.03	7.73	8.80	0.6	0.7	0.7
	Rosie	Crisp	TB	20/09/2017	33	6	0.4	0.6	0.6	58.63	58.13	28.13	28.40	8.83	8.27	8.47	9.20	0.6	0.6	0.6
	Sprite	Szczuka		20/04/2017	22	22	0.4	0.5	0.4	31.20	25.60	20.23	18.70	6.30	6.07	5.63	6.20	0.8	0.6	0.6
	Rudi	Finch	TB	27/02/2017	20	29	0.4	0.4	0.4	64.70	55.07	29.20	27.60	8.93	7.73	8.07	8.07	0.6	0.6	0.6
	Lexi	Munro	TBX	8/1/2016	17	18	0.5	0.8	0.5	52.03	50.07	27.03	26.23	8.37	8.03	7.57	6.97	0.8	0.6	0.6
	Tiny	Stenhouse		10/9/2015	20	15	0.6	0.5	0.5	56.20	54.60	27.27	27.43	8.50	8.60	7.90	7.80	0.8	0.7	0.8
						Average	0.45	0.62	0.47	52.25	48.05	26.32	25.49	8.15	7.79	7.56	7.84	0.70	0.63	0.65
						Standard Deviation	0.08	0.18	0.07	10.46	10.90	2.89	3.27	0.89	0.81	0.91	1.02	0.10	0.05	0.08
						Min	0.40	0.40	0.40	31.20	25.60	20.23	18.70	6.30	6.07	5.63	6.20	0.60	0.60	0.60
						Max	0.60	0.90	0.60	64.70	58.13	29.20	28.40	8.93	8.60	8.47	9.20	0.80	0.70	0.80
Moderate AR	Lordy	McGarry	TBX	16/08/2017	35	21	1	0.8	0.8	59.23	60.97	28.00	29.07	8.40	9.47	8.67	9.30	1.5	0.8	1.3
	Rudi	Barton	Warmblood	3/3/2017	34/35	23	1.7	0.8	0.8	61.23	58.20	28.23	27.97	8.90	9.17	8.57	8.93	1.2	1.3	1.3
	Rosie	Thompson	Irish Sp H	16/11/2016	43	16	1	0.6	0.6	58.93	58.73	27.67	28.00	8.63	8.17	8.80	7.23	0.9	0.7	0.9
	Pie	Baird	TB	25/07/2014	24	12	0.7	1.2	0.7	78.47	71.93	32.40	31.20	9.93	9.80	9.17	8.27	0.8	0.8	0.7
	Bessie	Fraser	TB	16/09/2015	17	14	1.0	1.1	0.6	69.90	64.83	30.37	29.93	9.33	8.83	8.90	9.27	1.1	0.7	1
	Hugo	McNaughton	hunter	29/06/2016	30	40	0.5	0.8	0.5	61.23	73.17	28.27	31.90	8.80	8.53	9.53	8.70	0.8	0.7	0.9
						Average	0.98	0.88	0.67	64.83	64.64	29.16	29.68	9.00	8.99	8.94	8.62	1.05	0.83	1.02
						Standard Deviation	0.37	0.20	0.11	7.11	6.00	1.69	1.50	0.50	0.55	0.33	0.71	0.25	0.21	0.22
						Min	0.50	0.60	0.50	58.93	58.20	27.67	27.97	8.40	8.17	8.57	7.23	0.80	0.70	0.70
						Max	1.70	1.20	0.80	78.47	73.17	32.40	31.90	9.93	9.80	9.53	9.30	1.50	1.30	1.30
Overall Average (not including endocarditis)							0.72	0.75	0.57	58.54	56.34	27.74	27.58	8.58	8.39	8.25	8.23	0.88	0.73	0.83
Overall Standard Deviation (not including endocarditis)							0.38	0.23	0.14	10.94	12.09	2.76	3.29	0.84	0.92	0.97	0.96	0.26	0.18	0.25

Measurement Summaries:

Measurement summaries based on AR degree, and associated graphs.

Diagnosis	Measurement	Commisural Measurement			Valve Area		Circumference		Diameter				Cusp Thickness		
		RCC/NCC	NCC/LCC	LCC/RCC	S	D	S	D	Systole		Diastole		Side		
									Front	Side	Front	Side	LCC	RCC	NCC
Normal	Average	0.46	0.42	0.42	49.19	51.67	25.50	26.63	7.86	7.41	7.78	7.43	0.59	0.60	0.59
	SD	0.05	0.04	0.04	6.95	5.03	1.90	1.24	0.62	0.69	0.52	0.73	0.06	0.07	0.06
	Min	0.40	0.40	0.40	38.30	38.90	22.40	23.40	6.70	6.30	6.60	5.90	0.50	0.50	0.50
	Max	0.50	0.50	0.50	62.10	57.90	28.70	28.40	9.00	8.70	8.60	8.30	0.70	0.70	0.70
Mild	Average	0.45	0.62	0.47	52.25	48.05	26.32	25.49	8.15	7.79	7.56	7.84	0.70	0.63	0.65
	SD	0.08	0.18	0.07	10.46	10.90	2.89	3.27	0.89	0.81	0.91	1.02	0.10	0.05	0.08
	Min	0.40	0.40	0.40	31.20	25.60	20.23	18.70	6.30	6.07	5.63	6.20	0.60	0.60	0.60
	Max	0.60	0.90	0.60	64.70	58.13	29.20	28.40	8.93	8.60	8.47	9.20	0.80	0.70	0.80
Moderate	Average	0.98	0.88	0.67	64.83	64.64	29.16	29.68	9.00	8.99	8.94	8.62	1.05	0.83	1.02
	SD	0.37	0.20	0.11	7.11	6.00	1.69	1.50	0.50	0.55	0.33	0.71	0.25	0.21	0.22
	Min	0.50	0.60	0.50	58.93	58.20	27.67	27.97	8.40	8.17	8.57	7.23	0.80	0.70	0.70
	Max	1.70	1.20	0.80	78.47	73.17	32.40	31.90	9.93	9.80	9.53	9.30	1.50	1.30	1.30
Endocarditis	Average	1.40	0.45	0.45	46.98	42.73	24.53	23.87	7.65	7.17	7.10	6.82	0.75	1.85	1.80
	SD	0.40	0.05	0.05	15.05	15.91	4.10	4.54	1.32	1.75	1.39	2.09	0.15	0.45	0.30
	Min	1.00	0.40	0.40	31.70	26.20	20.30	19.00	6.20	5.10	5.30	4.70	0.60	1.40	1.50
	Max	1.80	0.50	0.50	62.60	59.00	28.90	28.50	9.10	9.00	8.50	9.20	0.90	2.30	2.10

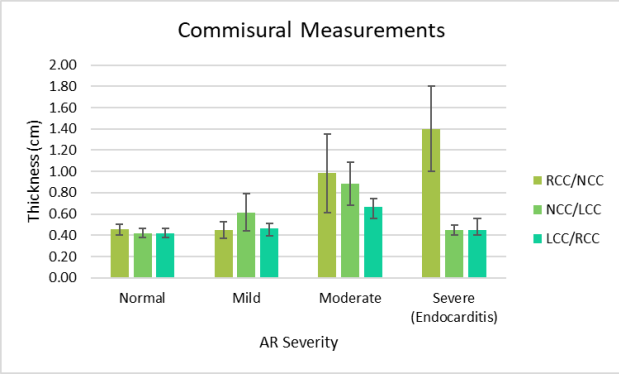

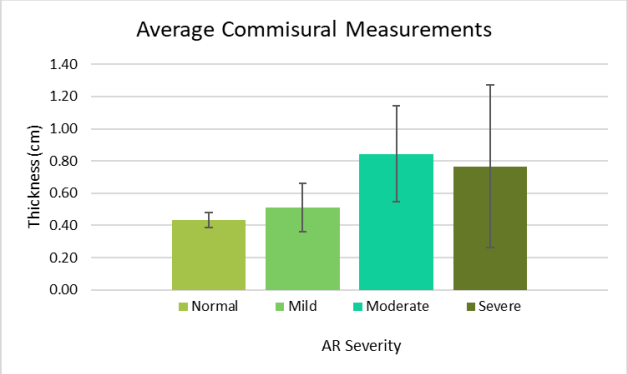

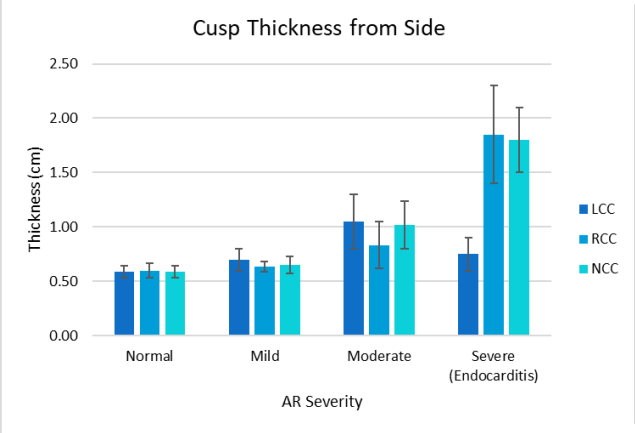

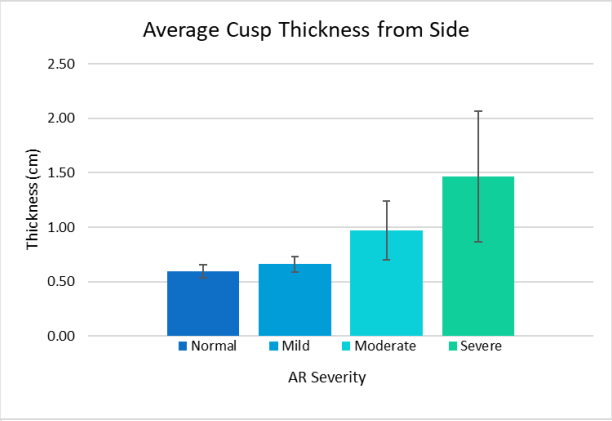

SAS Data:

Full data from SAS for statistical analysis of all measurements, both including and excluding severe AR cases.

With Severe AR Cases:

Analysis of Variance

Source	DF	Sum of Squares	Mean Square	F Value	Pr > F
Model	3	19.63666	6.54555	37.46	<.0001
Error	19	3.31987	0.17473		
Corrected Total	22	22.95652			

Variable	Parameter Estimate	Standard Error	Type II SS	F Value	Pr > F
Intercept	0.27546	0.59300	0.03770	0.22	0.6476
ncc	2.07319	0.23300	13.83382	79.17	<.0001
NCCL	2.03489	0.41649	4.17100	23.87	0.0001
DDS	-0.14659	0.08370	0.53605	3.07	0.0960

Bounds on condition number: 1.2831, 10.743

All variables left in the model are significant at the 0.1500 level.

Summary of Backward Elimination

Step	Variable Removed	Number Vars In	Partial R-Square	Model R-Square	C(p)	F Value	Pr > F
1	DDF	8	0.0000	0.8734	8.0038	0.00	0.9521
2	lcc	7	0.0001	0.8734	6.0115	0.01	0.9287
3	DSS	6	0.0009	0.8725	4.1027	0.11	0.7502
4	LCCR	5	0.0039	0.8685	2.5080	0.49	0.4918
5	VAS	4	0.0077	0.8609	1.2957	0.99	0.3334
6	RCCN	3	0.0055	0.8554	-0.1402	0.71	0.4104

Without Severe AR Cases:

Analysis of Variance

Source	DF	Sum of Squares	Mean Square	F Value	Pr > F
Model	2	11.22424	5.61212	30.18	<.0001
Error	18	3.34718	0.18595		
Corrected Total	20	14.57143			

Variable	Parameter Estimate	Standard Error	Type II SS	F Value	Pr > F
Intercept	-0.44490	0.31774	0.36457	1.96	0.1785
lcc	1.58185	0.46755	2.12858	11.45	0.0033
NCCL	1.82418	0.47408	2.75320	14.81	0.0012

Bounds on condition number: 1.4722, 5.889

All variables left in the model are significant at the 0.1500 level.

Summary of Backward Elimination

Step	Variable Removed	Number Vars In	Partial R-Square	Model R-Square	C(p)	F Value	Pr > F
1	LCCR	8	0.0000	0.7924	8.0001	0.00	0.9939
2	rcc	7	0.0005	0.7919	6.0287	0.03	0.8627
3	RCCN	6	0.0003	0.7916	4.0430	0.02	0.8985
4	DDS	5	0.0005	0.7911	2.0714	0.04	0.8524
5	DSS	4	0.0016	0.7895	0.1541	0.11	0.7424
6	CD	3	0.0038	0.7857	-1.6464	0.29	0.6000
7	VAS	2	0.0154	0.7703	-2.8280	1.23	0.2837